Improvement Strategies toward Stable Lithium-Metal Anodes for High-Energy Batteries
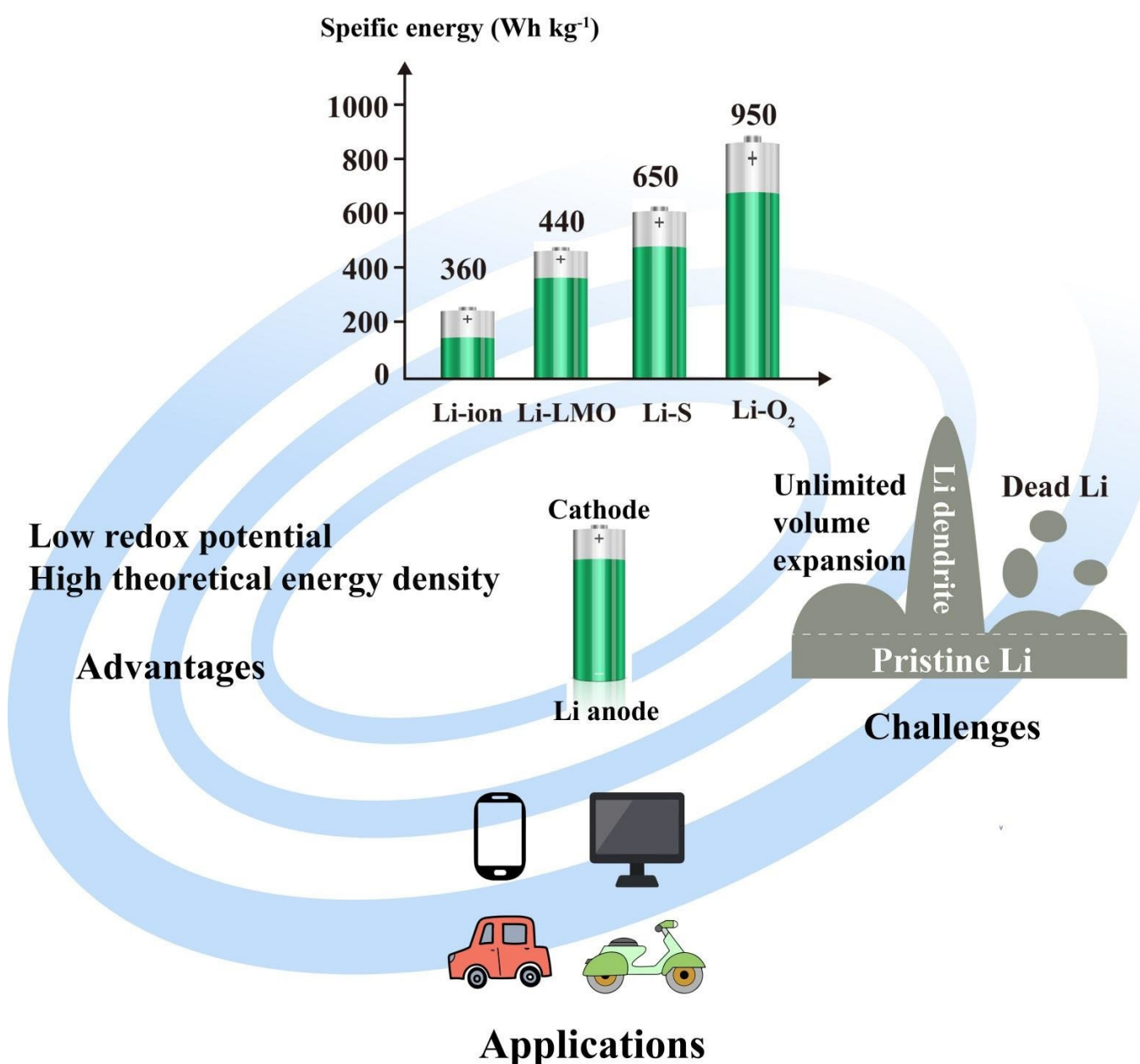
Jianhua Hou,*[a] Muyi Yang,[a] Bing Sun,*[b] and Guoxiu Wang*[b]

Lithium-metal (Li-metal) batteries are one of the most potential energy storage devices available these days. However, uncontrollable lithium dendritic growth and parasitic reactions lead to poor cycling efficiency and severe safety concerns, which restricts the use of Li-metal batteries in practical applications.

This article reviews the current development status of Li-metal anodes, including investigations of reaction mechanisms and performance improvement strategies. In addition, future opportunities for developing safe and high-performance Li-metal batteries are also outlined.

1. Introduction

Advanced energy storage technology is becoming a critical internal enabling force in modern societies. The increasing demand for rechargeable batteries in much broader applications requires us to develop new systems that are beyond the most cutting-edge lithium-ion batteries. In recent years, lithium-metal (Li-metal) batteries have attracted vast attention due to the high theoretical specific capacity (3860 mAh g^{-1}) and low electrode potential of Li-metal anodes.

The history of lithium metal batteries can be traced back to the first determination of the electrode potential of lithium in 1913,[1] but the high reactivity of lithium hinders the development of lithium metal batteries (Figure 1a). In 1975, the successful development of the Li/MNO$_2$ battery promoted rapid development in the research field of lithium metal batteries, such as the Li/MOS$_2$ battery.[2] However, due to the serious safety issues of lithium metal batteries, the research on lithium metal batteries temporarily stopped.[3] Subsequently, in the early 1990s, the safety issue caused by lithium dendrites was solved with the advent of rocking chair technology, which allowed lithium to exist in an ionic form rather than in a metallic state.[4,5] This facilitated the rapid development of lithium-ion batteries. Another technological breakthrough worth mentioning is the application of non-flammable solid polymer electrolytes (SPEs) instead of liquid electrolytes, which can fundamentally solve the safety problems caused by lithium dendrites, because the flammable organic solvent system electrolytes used in traditional lithium batteries is the origin that causes the safety issues.[6] In addition, in 1999, SPEs were successfully applied to lithium-ion batteries.[7] However, the development of SPEs was limited by their inability to provide sufficient ionic conductivity at room temperature.[8]

The anode material in traditional lithium-ion batteries was graphite. Research and development to extend the capabilities of this battery system have already reached a mature stage.[9–12] However, the low theoretical specific capacity of graphite materials, which is 372 mAh g^{-1}, is insignificant for high-energy

applications.[13] In recent years, Li-metal anodes have attracted vast attention due to its high (3860 mAh g^{-1}) theoretical specific capacity and low electrode potential. If we use Li-metal electrodes to replace graphite in lithium-based batteries, the specific energy of the rechargeable batteries will significantly increase. As shown in Figure 1(b), the specific energy of Li-metal batteries is much higher than that of lithium-ion batteries. By matching the lithium-metal anode with the spinel LiMn$_2$O$_4$ (LMO) cathode, the specific energy of the Li-LMO battery can be increased to about ~440 Wh kg^{-1}, while the specific energy bottleneck of lithium-ion batteries is 260 Wh kg^{-1}.[14] And in the lithium-sulfur (Li-S) batteries and lithium-oxygen (Li-O$_2$) batteries, the specific energy is increased significantly by up to ~650 and ~950 Wh kg^{-1}.[15] In terms of volumetric energy density, lithium-ion batteries can reach ~700 Wh L^{-1}, but lithium-air batteries can reach ~1100 Wh L^{-1}, and anode-free Li-batteries can reach 1200 Wh L^{-1}, possessing a high energy density that is difficult to achieve with lithium-ion batteries, and can even approach that of gasoline.[15,16]

As mentioned above, metallic lithium has exciting advantages as the anode material for high-energy rechargeable lithium batteries. On other hand, the high reactivity of lithium-based batteries makes them easily corroded by liquid electrolytes. Parasitic reactions with electrolytes generate a variety of inorganic products like Li$_2$CO$_3$, Li$_2$O, LiF, etc.[17] and organic products such as ROCO$_2$Li and ROLi (R is the alkyl functional group).[18] These parasitic reactions not only reduce the utilization rate of metallic lithium and electrolytes but also may generate an appreciable amount of gas, which is likely to cause safety problems for Li-metal batteries. In addition, the presence of lithium dendrites is another challenge that may further impinge on the safety of Li-metal batteries. Any uneven deposition or dendritic growth of Li-metal can cause severe issues.[19,20] As shown in Figure 1(c), both the unlimited volume expansion and dendrite growth of lithium will cause the surface of lithium anodes to become porous and loose, resulting in large amounts of "dead" lithium. In addition, it will lead to solid-state electrolyte interface (SEI) rupture and increased side reactions.[21–23] The SEI on the surface of lithium anodes in a Li-metal battery is a passive film formed by a reaction between the active lithium and organic electrolytes. Severe volume change can lead to the rupture and reconstruction of SEI on the lithium surface. The continuous reconstruction of SEI consumes extra electrolytes via increased side reactions, which greatly reduces the Coulombic efficiencies. Furthermore, it can lead to a significant increase in voltage polarization. Lithium dendrites and "dead" lithium cause the surface of the Li-metal to become porous and loose. The specific surface area and thickness of the SEI will increase as well, thereby increasing the

[a] *Prof. J. Hou, M. Yang*
     School of Environmental Science and Engineering
     Yangzhou University
     Yangzhou 225000, China
     E-mail: jhhou@yzu.edu.cn
[b] *Dr. B. Sun, Prof. G. Wang*
     Centre for Clean Energy Technology, School of Mathematical and Physical
     Sciences, Faculty of Science
     University of Technology Sydney
     Ultimo NSW 2007, Australia
     E-mail: bing.sun@uts.edu.au
          guoxiu.wang@uts.edu.au

Batteries & Supercaps

Review
doi.org/10.1002/batt.202200231

Chemistry Europe
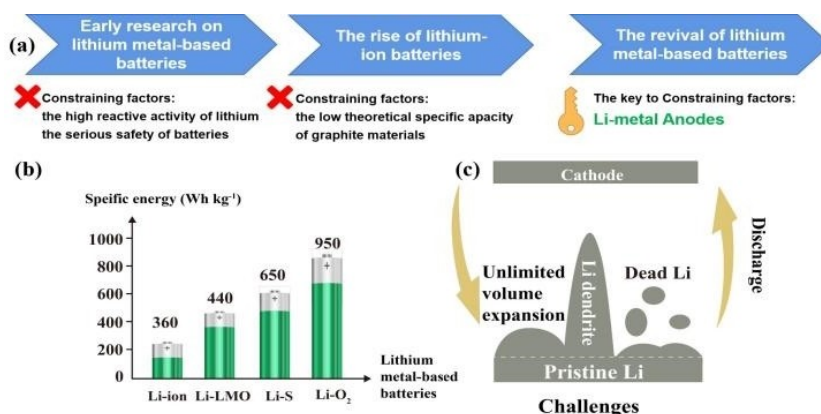European Chemical
Societies Publishing

Figure 1. a) The research history of lithium metal-based batteries. b) The comparison of specific energy between the traditional Li-metal batteries and Li-ion batteries. c) The main problems of Li anode in Li metal-based batteries.

diffusion path of Li$^+$, and any "dead" lithium will cause an increase in surface resistance. All these factors result in large polarization and low energy efficiency. Last but not least, safety issues should not be ignored. The continuous generation of lithium dendrites may increase stress on a cell separator membrane, and can eventually penetrate the separator and cause the battery to short-circuit, causing safety issues such as battery thermal runaway.[21–23] In short, the presence of lithium dendrites significantly affect the safety measures of Li-metal batteries, resulting in a reduction in Coulombic efficiency and shortened battery life. In summary, there are still many challenges in developing high-performance Li-metal batteries, and it continuously calls for understanding the reaction mechanism of Li-metal anodes as well as solutions to resolve those issues.[21–23]

Based on this, there is a need to develop lithium metal-based batteries with high energy density and guaranteed safety performance. Li-metal anodes are of great significance to the next generation of energy storage equipment. However, the development of practical Li-metal anodes was held up by the generation of lithium dendrites, which can cause various safety issues, such as uncontrollable thermal runaway, fire, and even explosions.[24,25] In addition, the unlimited expansion of Li-metal volume during repeated stripping/plating processes also induces severe issues such as powdering of Li-metal, consumption of electrolytes, and mass generation of gas.[26]

In recent decades, researchers have made great efforts to solve the above-mentioned safety issues. They developed a variety of approaches to reduce the outgrowth of lithium dendrites during electrochemical reactions, including adjusting the interface of Li-metal anodes,[27–29] optimizing electrolyte composition,[30–34] designing nano-structured Li-metal anodes,[35,36] and developing solid-state electrolytes.[37–39] Here, in this review, we summarize the existing challenges of Li-metal anodes, the evolution models of lithium dendrites, and the improvement strategies for Li-metal anodes. Besides, the relatively new point of environmental stability should be considered as a key issue for highly reactive lithium metal. Therefore, we also present the effects of air stability and temperature variations on lithium anodes and propose to counteract them accordingly. In addition, we discuss potential prospects for Li-metal anodes in practical applications.

2. Lithium Dendritic Growth Models

2.1. Charge-induced growth model

The uneven deposition of lithium ions can easily lead to the materialization of protruding lithium nuclei on the surface of metallic lithium. Ding et al.[40] proved that the tip of the lithium nucleus tends to accumulate many electrons due to the sharp point effect and thus has a higher local electric field. The local high electric field strength easily attracts more Li$^+$ which accumulates and grows as lithium dendrites. The addition of further cations forms an electrostatic shielding on the protrud-

Jianhua Hou is an associate Professor of Yangzhou University (YZU), China. His main research directions include synthesis, assembly and precise regulation of porous carbon materials and composite nanostructures, and the structure-activity relationship with battery performance. His current research focuses on lithium batteries and sulfur batteries, as well as the microscopic design of advanced electrode materials for green energy conversion and storage applications.

Muyi Yang is a postgraduate student of Yangzhou University, China. Her current research is related to advanced batteries, including rechargeable lithium-ion, sodium-ion, and potassium-ion batteries. Her research activities involve literature collation, characterizing fundamental materials properties, experiments to obtain key electrochemical performance data and the coordination of the research team's daily work.

Batteries & Supercaps

Review
doi.org/10.1002/batt.202200231

**Chemistry
Europe**
European Chemical
Societies Publishing

ing lithium nuclei, thereby inhibiting the rapid tip growth of lithium. The reduction potential of metal cation (M^+) additives in the electrolytes maybe evaluated by the following Nernst equation:

$$E_{red} = E_{red}^{\varphi} - \frac{RT}{zF} \ln \frac{\alpha_{red}}{\alpha_{ox}} \tag{1}$$

where, E_{red}^{φ} represents the typically reduced potential of the cation, R (8.314 $J\,mol^{-1}\,K^{-1}$) is gas constant, T is the experimental temperature, the number of electron transfer moles is given by z, and F is the Faraday constant (96485 $C\,mol^{-1}$), α_{red} and α_{ox} are the chemical activities of reducing agent and oxidizing agent, respectively. Therefore, by reducing the concentration of cationic additives in the electrolytes, the reduction potential of $E_{M^+/M}$ can be reduced to less as compared to the Li^+ reduction potential $E_{Li^+/Li}$ (For example, when the cationic additive concentration is 0.05 $mol\,L^{-1}$, and reduction potential $E_{Cs^+/Cs} = -3.103$ V, when the concentration is 1 $mol\,L^{-1}$, the reduction potential is -3.04 V). When the applied voltage V_a is higher than $E_{M^+/M}$ and lower than $E_{Li^+/Li}$, the metal cation M^+ will be attracted to the protruding lithium nucleus to act as an electrostatic shield, forcing Li^+ to deposit on nearby non-protruding positions.[40] To obtain a lithium deposition morphology free of dendrites, the charge-induced growth model provides significant guidance for solving the problem of lithium dendritic growth.

2.2. Space-charge model

Chazalviel et al.[41] presented the space charge model and gradually fine-tuned over time.[42,43] This model is mainly suitable for low-concentration electrolytes or rapid lithium deposition processes, and it is often applied to non-aqueous liquid electrolytes. In dilute solution, when lithium ions are deposited at high rates, the concentration of anion at the electrode surface will reduce. Anions are consumed near the electrode surface, generating a high space charge near the electrolyte/electrode interface, resulting in the branching growth of lithium deposition.[44]

Increasing the conductivity/migration number of cations or anchoring anions can alleviate the growth of lithium dendrites induced by the space charge. When a Li battery starts to discharge, Li^+ and anions migrate respectively to the anode and cathode under the driving force of the electric field. Li^+ can be inserted into the electrode materials of the cathodes. Without any electrochemical reaction, the anion concentration is only enriched near the surface of the anode, thereby generating a concentration gradient of anions. When the battery starts to charge, Li^+ and anions migrate to the anode and the cathode in opposite directions. The anions are enriched in the cathode area, while Li^+ ions accept an electron and reduce to metallic Li and are deposited on the anode. Chazalviel et al.[42] recognized a bipolar plate model to study the concentration changes of the micro-area at the surface of the lithium anodes. Agreeing with Fick's second law combined

with the boundary conditions, the following concentration gradient formula has been established on the surface of Li-metal anodes:[42,43]

$$\frac{\partial C}{\partial x}(x=0) = \frac{-J}{eD(1+\frac{\mu_c}{\mu_a})} \tag{2}$$

Here, J stands for current density, e for a charge, D for bipolar diffusion factor, and μ_c and μ_a for anions and cations migration numbers, respectively. Based on the above equation, the following two situations may occur:

In the first case, when $\partial C/\partial x < 2\,C_0/L$, the concentration gradient remains unchanged, indicating the ion concentration in the electrolyte reaches a steady state. The initial concentration of Li^+ is represented by C_0 in the electrolyte, and the electrode separation distance is L. In this situation, the concentration of anion in the anode is C_a ($C_a = C_0 - \Delta C_a$), and the concentration of Li^+ in the cathode is C_{Li+} ($C_{Li+} = C_0 + \Delta C_{Li}^+$). Therefore, the change on either side of the electrodes is:

$$-\Delta C_a \approx -\Delta C_{Li^+} = \frac{\mu_a}{\mu_a + \mu_{Li^+}} \frac{JL}{eD} \tag{3}$$

In the second case, when $\partial C/\partial x > 2C_0/L$, there is a big difference in ion concentration on the surface of the cathode and the anode. The concentration of Li^+ on the surface of the anode will be reduced to zero quickly, and an electronegative space charge zone will be formed, which further promotes the generation of lithium dendrites. With the formation of dendritic lithium, the polarization voltage increases significantly. The depletion time of Li^+ at the surface of Li-metal anodes is called the transition time (τ), generally referred to as "Sand's Time".[45] The value of τ can be calculated by the following equations:

$$\tau = \pi D [\frac{eC_0}{2Jt_a}]^2 \tag{4}$$

$$t_a \approx 1 - t_c = \frac{\mu_a}{\mu_a + \mu_c} \tag{5}$$

In the formulae, t_a and t_c represent the migration numbers of anions and Li^+, respectively. It is obvious that the value of τ is proportional to the square of the concentration of lithium salt in the electrolyte. In contrast, the current density is inversely proportional. Therefore, reducing the initial concentration of lithium salt and increasing the current density may promote the development of lithium dendrites. Chazalviel et al. also discovered that the concentrations of anions and Li^+ showed different effects on τ. When the concentration of anions in the anode area gradually decreases, the positive charge of the anode will be excessive, which will form a local net charge to generate an electric field, leading to the nucleation and growth of lithium dendrites. According to Equation (2), when $\partial C/\partial x$ starts to linearly change with the

Batteries & Supercaps

Review
doi.org/10.1002/batt.202200231

Chemistry Europe

European Chemical
Societies Publishing

current density J, the current density is the limiting current density at this moment.

$$J* = \frac{2eDC_0(\mu_a + \mu_c)}{L\mu_a} \qquad (6)$$

Exceeding this current density will cause dendrite growth. Furthermore, Chazalviel et al.[42] estimated that the growth rate of lithium dendrites would be v which correlates with the mobility of anions and the electric field strength:

$$\mathrm{v} = \mu_a E \qquad (7)$$

where E is the electric field strength.

2.3. The deposition-dissolution model

The deposition-dissolution model explains the processes producing dead lithium and the granular surface accumulation of lithium from the perspective of thermodynamics.[46] During Li-metal battery charging, the main processes of lithium deposition on the surface of the Li-metal anode are as described below:

At first, Li$^+$ migrates by the SEI film to deposit on Li-metal, and the SEI film is not damaged at this time.[46] The preferred lithium deposition point is associated with the mechanical stress of the SEI film, which makes the conductivity of lithium ions relatively high at the deposition point. This results in uneven lithium-ion flow and non-uniform lithium deposition. Besides this effect, the crystal defects and grain boundaries on the lithium surface will also promote uneven lithium deposition. And then, due to the effect of stress, the morphology of the deposited lithium will be deformed to relieve the stress.[46] Meanwhile, the deposition of lithium is limited by the surface tension of the Li-metal anode near the deposition point, the defects in SEI film, the surface crystal defects, and the lithium grain boundaries. The SEI film layer is damaged under the action of lithium growth stress, and the lithium further grows into whisker-like lithium.[46] In the last stage, bent lithium whiskers may break and dissolve at the junction, resulting in granular lithium and dead lithium under high current density or low-temperature conditions. It is easier to produce a large amount of dead lithium because the lithium whiskers are easy to break under such conditions. When considering the differences in the deformation stress of lithium dendrites caused by surface tension, the following formula is satisfied:

$$\Delta P = \gamma \ (1/R_1 + R_2) \qquad (8)$$

where ΔP is the difference in the deformation stress of lithium dendrites, the surface of lithium tension is represented by "γ", and R_1 and R_2 are the radii of curvature of the corresponding curved surfaces. Yamaki et al.[46] calculated and simulated a case where $\Delta P/\gamma$ is less than 0.2 μm^{-1}, wherein the damage to the SEI protective layer by dendritic growth can be suppressed.

2.4. Heterogeneous model

In addition to the space charge model described above, the heterogeneous model proposed by Ely et al.[47] is also a model that explores the lithium deposition process. Differing from the space charge model, the heterogeneous model is suitable for the primary stage of nucleation. The main theory of the heterogeneous model is introduced as follows. Lithium ions obtain electrons and are electroplated on the current collector. After a crystal nucleus is formed, the orientation of this crystal nucleus presents heterogeneous characteristics due to the influence of the substrate and impurities, which promotes heterogeneous nucleation. Heterogeneous nucleation is controlled by thermodynamics, so the nucleation of Li-metal can be enhanced by reducing the nucleation barrier. The nucleation behavior depends on the characteristics of the carrier (such as lattice matching and crystal structure, crystal plane orientation, and defects). When the lithium core continues growth to a critical size, it can reach a thermodynamic and kinetically stable state.[48] However, if the lithium nucleation rate is extremely fast, the lithium nucleus generated by the heterogeneous nucleation is morphologically unstable, and it easily forms dendritic lithium. Furthermore, due to the presence of heterogeneous interfaces, Li-metal extrusion caused by stress can cause lithium dendrites to grow.[49] The initial nucleation morphology shows a vital position in the later lithium deposition and growth processes. According to this model, formulae can be derived for the contact angle between the crystal nucleus and the electrolyte and the critical free energy, respectively:[47,50]

$$\mathrm{Cos}\,\theta = \frac{\gamma_{SE} - \gamma_{SN}}{\gamma_{NE}} \qquad (9)$$

$$\Delta G_{eq}^* = \frac{1}{3}(4\Pi r_{eq}^{*2})\gamma_{NE}(\frac{2 - 3\cos\theta + \cos^3\theta}{4}) \qquad (10)$$

where θ is the contact angle between the crystal nucleus and the electrolyte, and γ_{SE}, γ_{SN}, and γ_{NE} are the free energies of the interfaces of the substrate/electrolyte, substrate/nucleus, and nucleus/electrolyte, respectively. When the contact angle $\theta = 0°$, the free energy of nucleation is 0; when $\theta = 180°$, the required free energy of nucleation is the same as the energy required to achieve uniform nucleation. The contact angle can be reduced by increasing the wettability between the lithium nucleus and the conductive substrates, thereby reducing the free energy of nucleation. This could explain why the type of the substrate has such a significance on lithium nucleation behavior.

These different models help to understand the nucleation and growth behavior during lithium deposition process. The heterogeneous model describes the early nucleation behavior on the current collectors, which can guide the design of lithium hosts to suppress lithium dendrites. In contrast, the equations of the space-charge model emphasize that the lithium ion distribution directly affects the reactivity of different sites.[51]

Batteries & Supercaps

Review
doi.org/10.1002/batt.202200231

Chemistry Europe
European Chemical
Societies Publishing

Therefore, strategies such as decreasing the effective local current density, increasing the lithium salt concentration in the electrolyte, and increasing the lithium ion migration number are beneficial for achieving the inhibition of lithium dendrites. The deposition-dissolution model addresses the mechanism of lithium deposition and reveals that lithium whisker growth occurs from the base. In addition to the main dendrite growth models introduced above, there are phase field models,[52] surface nucleating and diffusion models,[53] etc. An in-depth understanding of dendrite growth models can assist researchers in furthering their research into novel techniques for addressing the problem of lithium dendrite formation.

3. Characterization Techniques for Li-metal Anodes

Lithium dendrites have always been a major problem hindering the development of Li-metal batteries. With the continuous development of advanced characterization technologies, a variety of technologies have been applied to research on Li-metal anodes. These characterization technologies can be divided into two categories.[23] One category detects the morphology and structure of lithium metal, atomic force microscopy (AFM), nuclear magnetic resonance (NMR), scanning electron microscopy (SEM), and transmission electron microscopy (TEM) etc. are among these methods. The other

category uses the detection of Li-metal anode surface chemistry, such as XPS (X-ray photoelectron spectroscopy)), FTIR (Fourier transforms infrared spectroscopy), and atomic emission spectrometry (AES). In addition, applying X-ray diffraction to characterize the dendrite enlargement of lithium has been reported.[54]

SEM is a conventional characterization method, which can be used to observe the surface and cross-sectional morphologies of Li-metal anodes.[55] It can also provide a detailed comparison of the effectiveness of electrode surface modification.[56] In addition, SEM with a focused ion beam (FIB) can be used to cut specimens, and SEM with X-ray energy dispersion spectroscopy (EDX) can be used to conduct elemental analysis.[57] With the help of SEM, Lu et al.[58] succeeded in making Li-metal batteries charged and discharged efficiently by employing liquid electrolytes. After 100 cycles at 0.5 C charge/discharge and 0.2 C charge/1 C discharge, a cross-sectional SEM pictures of the Li anodes were produced from the cells are shown in Figure 2(a and b). After 100 cycles, battery failure during fast charging was found to be not necessarily due to dendrite growth and short circuits. Instead, it was also possible that the anode side was continuously corroded by the electrolyte, resulting in a passivating layer of "dead" lithium with a thickness of more than 100 μm. At the same time, a large amount of electrolyte is consumed, which causes the internal impedance of the battery to increase and eventually leads to failure. The characterization results exhibited that the higher the charge-discharge rate, the
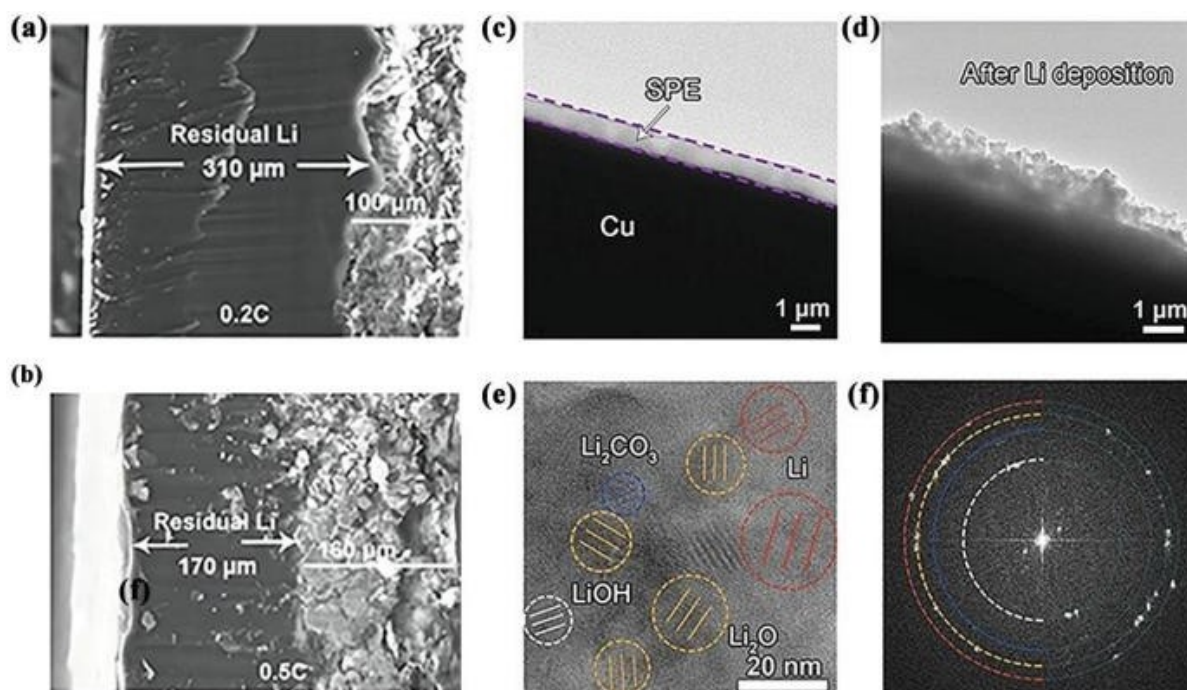

Figure 2. Cross-sectional SEM images of the Li anodes after 100 cycles at a) 0.2 C charge and 1 C discharge, and b) 0.5 C charge and discharge, respectively. Reproduced with permission from Ref. [58]. Copyright (2014) Wiley-VCH. c) TEM images illustrating morphological change before Li deposition. d) TEM images illustrating morphological change after Li deposition. The layer between the purple lines is identified as the solid polymer electrolytes (SPE). e) Recognized crystalline grains of Li metal, Li_2O, Li_2CO_3, and LiOH in the interface. f) The corresponding FFT of (e), red circle: Li, 2.48 Å, yellow circle: Li_2O, 2.66 Å, blue circle: Li_2CO_3, 3.02 Å, white circle: LiOH, 4.35 Å. Reproduced with permission from Ref. [67]. Copyright (2020) Wiley-VCH.

Batteries & Supercaps | Review
doi.org/10.1002/batt.202200231

Chemistry
Europe
European Chemical
Societies Publishing

thicker the dead lithium passivation layer and the less active lithium remains.[58] Their work has enhanced our understanding of Li-metal batteries. In addition to the study of Li-metal anodes in liquid electrolytes, SEM has also been used in research on Li-metal anodes with solid-state electrolytes. For solid-state batteries, it is difficult to directly observe growth and nucleation, process of Li-metal, because of the complexity of preparing samples and the lack of characterization apparatus. The interface formed in situ between the Li-metal and solid-state electrolyte anodes during charging and discharging makes it difficult to separate anodes without damage during sample preparation. Therefore, most of the ex-situ characterization methods applicable to liquid electrolytes are not applicable to solid-state electrolytes.[59] Non-destructive testing would provide more accurate information about the interior of the battery and improve the reliability of battery testing methods. However, in-situ nondestructive characterization methods cannot observe the evolution of the front of the two-dimensional plane because the inorganic solid-state electrolyte is opaque, resulting in a big challenge for non-destructive in-situ characterization. SEM on suitable open samples provides an in-situ characterization method that can be applied to solid lithium anodes. Westover et al.[60] observed the growth process of lithium dendrites in lithium phosphorus oxide nitride (a solid lithium anode) using an optical microscope. Li et al.[61] used in-situ SEM to study the steps of lithium dendrites penetrating LLZO electrolytes. They found that metallic lithium would form large voids due to uneven deposition and huge volume changes occurred at the flat electrode interface on the deposition side, while lithium dendritic growth starts on the deposition side.

TEM is often used to observe the morphologies of Li-metal anodes. It has been found when using TEM to observe metallic lithium at room temperature, that the high-intensity electron beam current will inevitably damage the physical and chemical state of Li-metal, causing the final observed results to deviate from the original situation.[62–64] Therefore, some researchers have turned their attention to cryo-electron microscopy (cryo-EM), to protect the unstable metallic lithium via low temperature. This low-temperature protection strategy has been successful, and it can also be used in the characterization of solid-state electrolytes. However, TEM at room temperature can detect the deposition and dissolution behavior of Li-metal in situ, which is not possible with cryo-TEM.[65,66] Sheng et al.[67] used cryo-TEM to explore the influence of the SEI layer on the morphology of lithium deposition in the poly(ethylene oxide) (PEO) solid-state electrolyte system. The TEM images illustrating morphological change before and after Li deposition are shown in Figure 2(c and d). Figure 2(e) is an HRTEM image of the interface, and Figure 2(f) is the corresponding FFT of 2e. It can be seen that after adding Li_2S to SSE, more LiF phases appeared in the interface layer. Analysis shows that Li_2S as an additive can accelerate the formation of LiF, and nano-scale LiF crystals can effectively increase the ion diffusion rate and prevent the continuous side reaction between PEO and metallic lithium.[67] As a result, a stable negative electrode interface is constructed,

which can homogenize lithium deposition and hinder the formation and growth of dendrites.

AFM characterization not only reads the morphological and surface mechanical properties of the specimens but can also detect the distribution of electronic conductance by using the Peak Force Tunneling mode.[68] It is worth mentioning that Huang et al.[69] combined AFM and ETEM (environmental transmission electron microscopy) to observe and analyze the whole process of lithium whisker nucleation, growth and collapse in situ. They found that the stress generated during the growth of lithium dendrites is as high as 130 MPa and the yield strength of lithium dendrites is as high as 244 MPa. This research established an effective dynamic in-situ experimental characterization technique for studying lithium dendrites, and accurately measured the mechanical properties and force-electric coupling characteristics of lithium dendrites. It includes a scientific foundation for the development of high-capacity, long-life solid-state Li-metal batteries. Nuclear magnetic resonance (NMR) detects the changes in the nuclear spin states induced by an external magnetic field and is a non-destructive analysis method. For example, two-dimensional lithium-ion exchange NMR can be employed to investigate lithium-ion transport behavior at the interface of solid-state electrolyte/electrode.[70] Both NMR and general magnetic resonance (MR) techniques can provide quantitative information on battery materials without damage. Although NMR cannot penetrate bulk lithium, it can characterize thinner microstructures such as lithium dendrites near the interface and electrolyte.[71]

4. Strategies to Improving Li Metal Cycle Life

4.1. Conductive three-dimensional framework

Conductive three-dimensional (3D) frameworks are an effective product of nano interface engineering. The principle of this approach is to build a layer of "scaffolding" between the SEI film and the metal lithium anodes.[23] The "scaffolding" needs good chemical stability and mechanical strength and the ability to allow lithium ions to pass through. During charging and discharging, the "scaffolding" can move with the SEI film to prevent the SEI film from rupturing and inhibit the generation of lithium dendrites. Li-metal anodes can show unlimited volume expansion due to their lack of matrix conversion reactions. In the past, some cost-effective strategies such as "microneedle surface treatment" technology have been used. The holes created by this strategy are "designed defects" in a lithium surface. Through these holes, the goal to allocate and partially refer to lithium plating and peeling processes can be implemented.[72] But this technology has certain limitations. Initially, the lithiation capacity of this technology was lower than expected. The Li deposition mode may change to dendritic development when the amount of Li deposited surpasses the volume of the holes. In addition, in the long cycle test, Li powder electrodes and Li foil electrodes with microneedle surface treatment will not fully store their total loading of Li. After several cycles, lithium powder and microneedle

Batteries & Supercaps

Review
doi.org/10.1002/batt.202200231

Chemistry Europe
European Chemical
Societies Publishing

lithium are transformed into 2D lithium foil, which then cannot suppress the generation of Li dendrites. In response to this problem, researchers have designed various conductive 3D frames to store Li-metal. First of all, compared with the two-dimensional copper foil collectors, 3D structures can improve the surface area of anodes. Meanwhile, conductive properties can reduce the local current density of the anode, thus mitigating the growth of Li dendrites.[73] Secondly, a high specific surface area may lead to low local electric fields, which can facilitate homogenous lithium deposition.[74] In a sub-micron conductive framework, electric fields are roughly uniform, and the charge is evenly dispersed. Eventually, a uniform Li surface will be formed, which will be further beneficial to the lithium electroplating process. At present, many conductive 3D frameworks have been developed, including carbon nanotubes, graphene, carbon nanofibers, porous metal composite matrix, and so on.[75] The following sections summarize the main 3D matrix framework strategies that have been studied in recent years to understand their design principles and reaction mechanisms.

4.1.1. Graphene composite matrix

In recent years, graphene, a two-dimensional material with various unique properties, in energy storage technologies, became one of the most preferred electrode materials, owning to its high electronic conductivity, stable structure, low density, and easy doping.[76] Based on these advantages, graphene can also be applied as a structural matrix to optimize Li-metal anodes.[77,78]

Cui et al.[79] first coated formulated lithium alloy (Li_xM) nanoparticles with graphene (<10 layers) materials having excellent hydrophobic properties and lower gas permeability. They then applied lithium alloy/graphene anode materials into a lithium battery with $LiFePO_4$, V_2O_5, or S as cathode materials, and used Li-metal anodes and graphene anodes for reference experiments. The electrochemical performance of their batteries was tested at high current densities, and the anode materials were observed via SEM, TEM, and XPS to confirm the flexibility, strength, and hydrophobic properties. The results show that batteries with lithium alloy/graphene as anodes can still maintain 98% of their initial capacity after 400 cycles of charging and discharging at a high current density. The main reasons are as follows: Firstly, Li_xM alloy materials can effectively tolerate volume expansion during the delithiation/lithiation processes. Secondly, the coated graphene material had superior hydrophobic properties and lower gas permeability and improved the stability of the anodes (to prevent parasitic reactions with residual air, moisture, and electrolytes). Moreover, for lithium-sulfur batteries, coated graphene materials inhibited the reaction of poly sulfur compounds with the Li-metal anodes. The coated graphene materials also reduced the loss of positive sulfur active material and maintained battery cycling stability. Li_xM nanoparticles were embedded in the graphene sheets, which gives the material good chemical stability, including excellent hydrophobicity and low gas

permeability. Meanwhile, the composite material shows good flexibility. Furthermore, this material can be easily mass-produced.[79]

Lai et al.[80] reported a hierarchical 3D porous silver-nano-wire-graphene framework (3D-SGF for short). This unique "layered binary stent" provides an ultra-fast, continuous and smooth electronic transmission channel. More importantly, this 3D frame displays higher flexibility and mechanical strength, which can buffer volume expansion during the successive processes of Li deposition/dissolution. As metal oxides can carry out redox reactions with metallic lithium, Yu et al.[81] successively modified a variety of metal oxide nanosheets (such as MnO_2, Co_3O_4, SnO_2) on graphene foams. The advantage of this method is that it can combine the advantages of both graphene foam frameworks and metal oxides. The graphene foam framework has the effect of limiting the volume expansion of lithium and stabilizing the electrolyte/electrode interface. The metal oxide nano-sheets can improve the lithium affinity of the framework, lower the local current density, as well as simultaneously induce the subsequent deposition of lithium ions and nucleation. In addition to the above-mentioned schemes, there are lots of other applications of graphene matrices to Li-metal, such as the influence of heteroatom-doped graphene on lithium deposition,[82–84] the application of nanoporous graphene to the matrix of molten lithium to optimize metal lithium anodes,[85] and so on.

In recent years, due to their simple preparation procedure, research on carbon nanotubes (CNTs) has also made considerable progress. Zhang et al.[86] reported a lithiophilic-lithiopho-bic gradient (LLG) strategy by adding CNTs and ZnO. Even at a high current density of $5\ mA\,cm^{-2}$, their technology may significantly decrease dendrite formation and provide ultra-long-term steady lithium dissolution/deposition. Wang et al.[87] first synthesized carbon nanotube (CNT) cluster balls by spray drying and then infiltrated an appropriate amount of molten lithium into the CNT powder matrix at high temperature to form a new type of composite framework called Li-CNTs. Studies have shown that the specific surface area of Li-CNTs is $55.6\ m^2\,g^{-1}$, which is three orders of magnitude higher than pure Li-metal anodes. The material's high specific surface area decreased the local current density on the electrode surface, and CNTs cluster spheres can effectively suppress the volume expansion of lithium, inhibit the growth of lithium dendrites, and the generation of dead lithium, resulting in more excellent electrochemical performance. CNT "paper" functioned as a high mass loading host for Li metal. CNT paper is strong and extensible and can withstand large volume changes. Ji et al.[88] designed and prepared a CNT paper matrix to accommodate lithium. This free-standing and lightweight framework can be injected with molten Li-metal, and it shows quite strong mechanical stability and high electronic conductivity. The surface of 3D Li/CNT electrodes with high conductivity has sp^2-hybridized carbon expandable 1D CNT and uniform Li loading, which can efficiently prevent the construction of Li dendritic crystals and preserve stability after long cycles at $10\ mA\,cm^{-2}$.

Batteries & Supercaps

Review
doi.org/10.1002/batt.202200231

Chemistry
Europe

European Chemical
Societies Publishing

4.1.2. Carbon fiber composite matrix

Due to their stable 3D networks, excellent electronic conductivity, and high specific surface area, self-supporting carbon fiber-based frameworks was widely exercised as current collectors for lithium deposition. For instance, graphitized carbon fibers,[89] 3D porous carbon fibers,[90] and carbon fiber cloth[91,92] have been intensively investigated recently.

Luo et al.[93] established a novel 3D framework with Mo_2N-modified carbon nanofiber (CNF) as Li host by a simple preparation method. The deposition of Li ions formed needle-like dendrites on a Cu foil. When using a bare CNF substrate, the isolated deposition of Li can be limited due to the reduced local current density in the 3D conducting framework, but it is impossible to achieve uniform distribution of Li nuclei and homogeneous Li deposition by relying only on the less lithophilic CNF substrate. However, due to the good lithiophilicity of MO_2N, the $MO_2N@CN$ substrate processes abundant nucleation sites and obtains ultra-low Li nucleation overpotential, which effectively promotes the uniform formation and deposition of Li nuclei, inhibits the Li dendrites and alleviates the volume expansion. Thus, the Coulombic efficiency has been significantly improved by about 99.2 %. The symmetrical cell with $Mo_2N@CNF$ substrate is stable for over 1500 h at 6 mA cm^{-2} for 6 mAh cm^{-2}. This work provides a new idea for the simple design of three-dimensional lithiophilic substrate for dendrite-free lithium metal anodes. Based on this work, the design of 3D lithiophilic hosts has been of interest to researchers. Liu et al.[94] reported on in-situ nitrogen-doped graphite carbon foams (NGCFs) being used as a lightweight and flexible current collector for Li-metal batteries, achieving uniform nucleation and growth of metallic lithium, effectively improving their electrochemical performance. The nitrogen-containing functional groups promote uniform lithium-particle growth at a low nucleation over potential. The initial lithium nucleation seed layer makes the growth of lithium more regular and suppresses the production of lithium dendrites in the initial state. In addition, the characteristics of high specific surface area, 3D porous framework, and lightweight reduce the local current density, avoid drastic changes of volume during cycling, and attain increased capacity.

Carbon fiber cloth (CFC) can maintain a stable fiber structure during a high-temperature lithium infiltration process and has been widely used as the carrier of composite Li-metal anodes recently.[72,95] Zhou et al.[96] used the classic electrochemical deposition method to directly form a CFC@Li composite anode on 3D CFC. The morphology changes in different Li metal anodes and the fabrication process of the CFC@Li anode are shown in Figure 3(a). Compared with other methods, this lithium-based composite preparation process is more controllable and can achieve uniform deposition of lithium without unwanted accumulation on the electrode surface.[96] Meantime it is also easy to mass-produce. They first oxidized the CFC and introduced oxygen-containing groups like hydroxyl and carboxyl groups on the surface. These surface functional groups helped induce uniform deposition of metallic lithium and formed a stable SEI film in situ on the electrode

surface. Under different lithium insertion capacities, metallic lithium is preferentially deposited on the surface of the CFC, gradually filling the holes in the 3D structure. The observed volume change during the lithium deposition process is relatively small. By using SEM observation, they found that the surface of the Li-metal was flat and uniform, and no dendrites were produced after multiple cycles. At the same time, they investigated the composition and stability of SEI films on the Li-metal surfaces by X-ray photoelectron spectroscopy. With oxidation-treated 3D CFC as the substrate, the SEI film formed during the metallic lithium deposition process contains multiple components such as lithium sulfide and lithium nitride, which promotes a good balance between lithium-ion diffusion and uniform deposition of metallic lithium. It maintained good stability during subsequent cycles. Based on the above experimental results, the surface of the CFC@Li composite anode prepared from the 3D CFC by the electrochemical deposition method had stable SEI films, which have good resistance to the growth and volume expansion of lithium dendrites.[96] This in-situ SEI composite 3D Li-metal protection strategy can prepare a Li-metal anode that is stable under high-rate conditions. Such Li-metal anodes can be matched with different positive electrode materials to assemble a full battery, showing excellent high-current charge and discharge capabilities and cycle stability. This kind of Li-metal composite anode has a simple manufacturing process and low cost and is estimated to become a promising applicant for a new generation of higher power battery materials. Besides, metal oxides such as SnO_2,[97] RuO_2,[98] Co_3O_4[99] and ZnO[100–102] have also been reported to improve the lithium affinity of carbon fibers and regulate the deposition process of lithium ions. To further promote the practical application of composite Li-metal anodes, Go et al.[102] created nano-cracks in CFC to improve the lithium affinity of the matrix, and then prepared a large-scale composite electrode of alkali metal/carbon composites. The manufacturing process of this composite material is shown in Figure 3(b). As shown in the figure, lithium or nanometals are first injected into commercial carbon cloth to form an alkali carbon/metal composite. They then successfully injected alkali metals by introducing nano-cracks in the carbon cloth through heat treatment. In this way, the stable electrochemical tripping performance of the battery has been realized. Compared to pristine copper electrodes, the composites prepared from this carbon cloth are capable of long-term cycling and are not hindered by alkali metal dendrite construction. In addition, this method injects the alkali metal into the carbon cloth quickly and directly, allowing for the large-scale production of composite electrodes.

The 3D structure of carbon fiber may have a lower current density, decrease the over potential for lithium nucleation, and limit the volume expansion of Li-metal. Therefore, designing suitable porous polar electrode materials to solve the problems of sulfur cathodes and lithium anodes in lithium-sulfur batteries merits more attention.
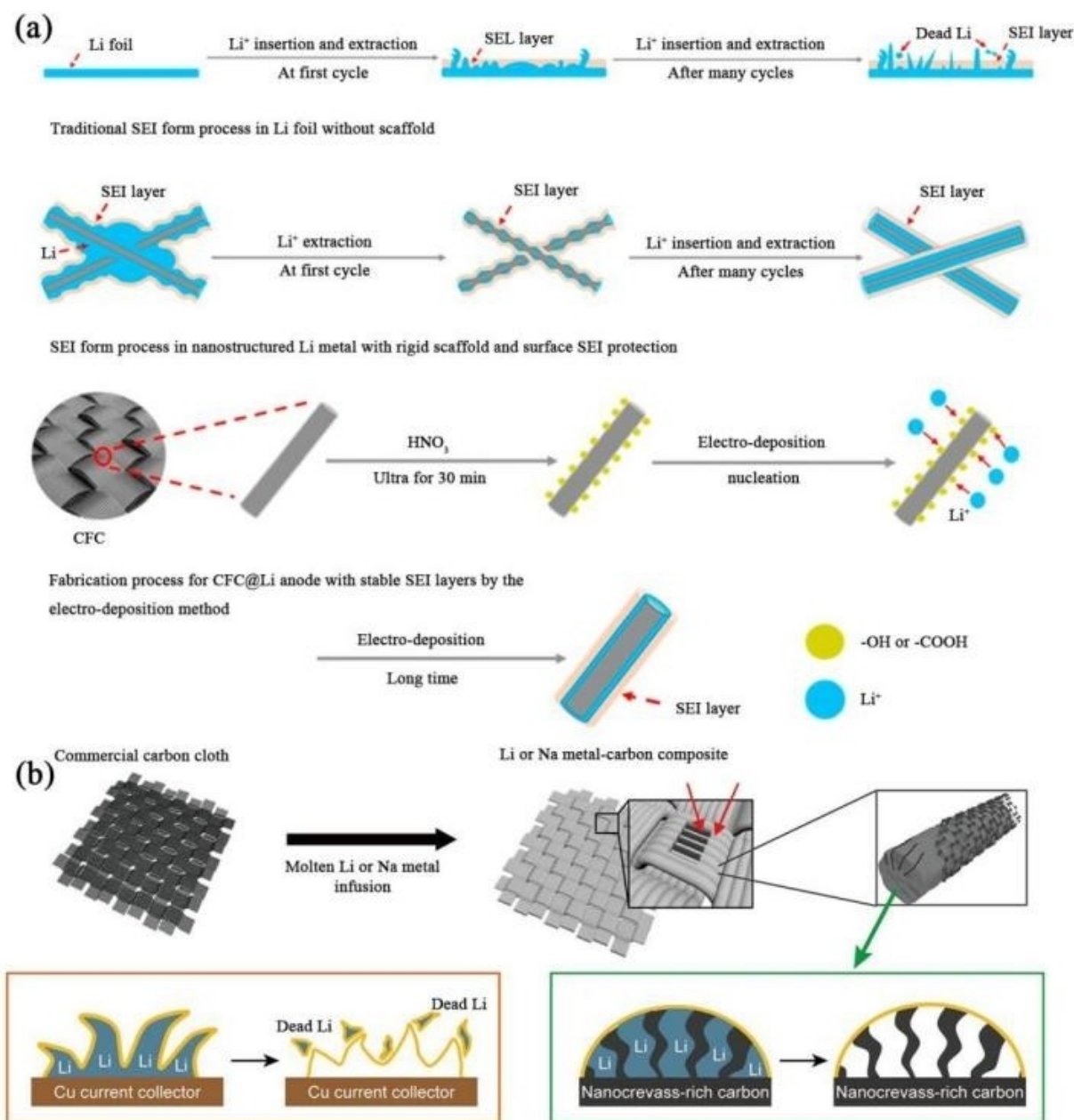
Figure 3. a) Schematic of the morphology changes in Li metal anodes and the fabrication process of CFC@Li anode. Reproduced with permission from Ref. [96]. Copyright (2018) Elsevier B.V. b) Schematic showing the fabrication process of the Li and Na metal/carbon composites. Reproduced with permission from Ref. [102]. Copyright (2018) American Chemical Society.

4.1.3. Porous metal composite matrix

Due to high electronic conductivity and structural stability, metal substrates are often used as current collectors for supporting electrode materials.[103–105] Therefore, 3D porous metal matrices have also been explored to use for a pre-stored lithium matrix or as the current collector for lithium electro-deposition. In this way, the volume expansion of Li-metal can be limited, and the deposition behavior of lithium ions regulated.[106–109] Designing a composite current collector to make full use of the advantages of different structures will be a major future direction for Li-metal carrier research.

Chi et al.[110] first proposed the application of nickel foam as a 3D matrix to accommodate lithium. The composite electrode they prepared has extremely high stability and excellent electrochemical performance. The protruding structures on the surface of the nickel foam can regulate the deposition of lithium ions and reduce the growth of lithium dendrites. Inspired by this design strategy, other modified metal foams were further developed and explored.[111–116] The schematic diagram and the corresponding optical photograph of Li-Ni composite lithium anode preparations are shown in Figure 4. Symmetrical cells assembled with these composite anodes can maintain a stable voltage platform (200 mV) after 100 cycles,
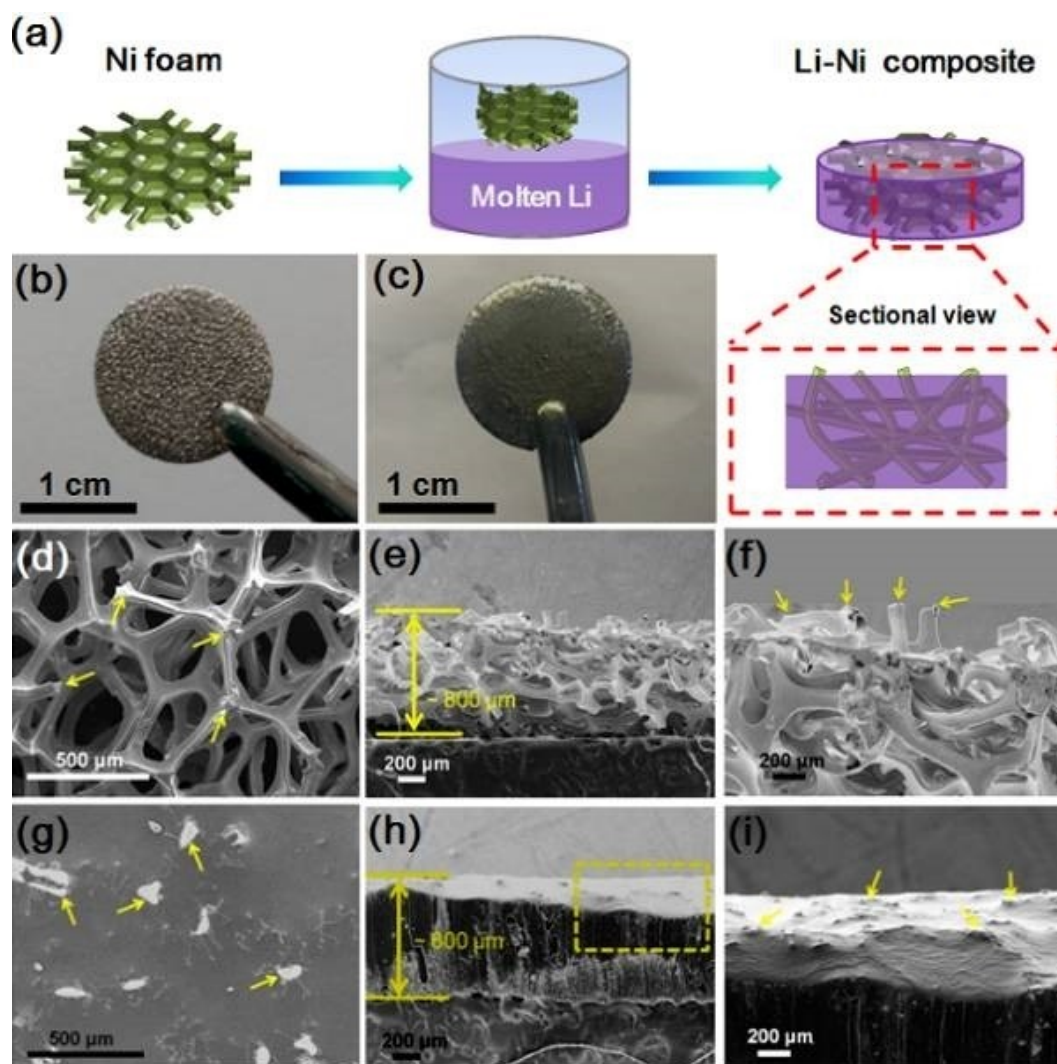
Figure 4. Preparation and SEM image of Li-Ni composite lithium anode. a) Schematic diagram of the preparation process of Li-Ni composite lithium anode. Corresponding digital camera images of b) the Ni foam and c) the Li-Ni composite. SEM images of the d–f) Ni foam and g–i) Li-Ni composite anode. Reproduced with permission from Ref. [110]. Copyright (2017) Wiley-VCH.

reflecting the dendrite-free property of Li-metal anodes and the low impedance characteristics of the interface. Moreover, after matching a Li-Ni composite lithium anode with a lithium iron phosphate (LFP) or lithium titanate (LTO) cathode, the resultant battery shows improved electrochemical performance compared with pristine Li-metal anodes. It demonstrates higher rate performance, better cyclic stability, and lower interfacial impedance. Also, mechanism studies have shown that the application of the 3D framework has played two roles. On the one hand, it provides sufficient space for pre-storing lithium during the preparation process. On the other hand, during the battery cycles, the three-position framework provides a carrier for receiving metallic lithium and can balance lithium ions and distribute electrons evenly. Their research provides a new design idea for the development of high-performance Li-metal anodes and dramatically promotes the application of Li-metal anodes.[110]

Although the 3D porous electrode has promoted the development of the protection of Li-metal anodes, there are some inherent shortcomings of such 3D porous electrodes. For instance, weak points include high inherent material density, non-lipophilicity, uncontrollable pore volume, and inability to be prepared in large quantities, significantly limiting their development for practical application. Based on this, Li et al.[117] proposed a large-scale slurry coating method to prepare a lightweight and lithiophilic conductive 3D collector called CCP-mix electrodes. In this study, micro-copper particles and nano-copper particles were used simultaneously to construct a conductive substrate. Sodium chloride was used as a pore former to make the electrodes porous. Copolymerized poly-acrylonitrile-polyacrylic acid (PAN-co-PAA) was used as a binder. Multi-walled carbon nanotubes and polyvinylpyrrolidone were used as conductive additives and copper particle dispersants, respectively. They directly mixed the above-mentioned raw materials in N-methyl pyrrolidone solvent in a

Batteries & Supercaps

Review
doi.org/10.1002/batt.202200231

Chemistry
Europe

European Chemical
Societies Publishing

certain proportion and then coated the materials on a commercial copper foil. After drying-washing (washing off the pore former-sodium chloride)-drying-low temperature heat treatment (Ar/H$_2$), the final lightweight porous lithiophilic conductive current collector (CCP-mix electrode) can be obtained. In the low-temperature heat treatment process, the nano-copper particles can be used as a sintering aid for the micro-copper particles to promote the formation of a conductive network with higher mechanical strength. In addition, the copolymerized polyacrylonitrile-polyacrylic acid (PAN-co-PAA) forms a porous structure with excellent lithiophilicity, forming a skeleton coated by copper particles and its upper layer is a lithiophilic carbon layer with a thickness of about 10 nm.[117]

Nanowire structured material can also play the role of confining lithium and homogenizing ion currents because of its large specific surface area and one-dimensional structure.[6] Yang et al.[118] used the redox method to construct 3D submicroporous copper nanowires on the surface of Cu current collectors for lithium deposition and storage. Inspired by this, the method of designing an active area with a porous structure on the surface of the current collector is now widely used to regulate the deposition and storage of Li-metal during lithium-ion flow, such as in 3D vertical Cu microchannel structure[119] and the lithiophilic CuO-Ni nanowire structures,[120] 3D porous copper, etc.[121] Besides these materials, other materials that form alloy compounds with lithium can induce lithium nucleation and promote rapid transfer of lithium ions. In this area, research on LiAl,[122] Li$_x$Si,[123] Li$_x$Zn,[124] Li$_x$Sn[125] and other alloy compounds formed with lithium has flourished.

In summary, it can be seen that the major design strategies for metallic current collectors focus on two approaches. One is to design a porous structure to increase the electrochemically active area of the surface and increase the space for lithium storage; the other is to modify the metal matrix with an alloy layer or a lithiophilic compound, which can induce uniform lithium nucleation and homogenous lithium-ion flow. For the future development of porous metal composite matrices for Li-metal anodes, we should focus on these two research directions.

4.1.4. Metal organic framework material

As is widely agreed, it is difficult to solve the problem of lithium dendritic growth and large volume changes to achieve long service life Li-metal anodes by using only a single strategy. Designing nanostructured current collectors and making full use of the advantages of different composites is a promising future direction for Li-metal research. A composite lithium carrier with a high ion conductive interface layer and a 3D current collector could be an ideal anode structure.[126] Metal-organic framework materials (MOFs) have been widely used in catalytic and energy storage materials, prompted by their attractive coordination methods and morphological structures.[127] The metal-organic framework (MOF) is self-assembled by organic ligands and metal ions. Structure

diversity, robust mechanical strength, tunable porosity, facile ion transmission and electronic insulation are just a few of the unique qualities of these materials, which makes them a preferred material for coatings. In addition, the large-scale synthesis and preparation process of MOFs is relatively simple, and composite Li-metal anodes can be prepared on a large scale. Zheng et al.[126] deposited lithium into a self-supporting conductive 3D framework to prepare a composite Li-metal anode with a small volume change. They combined a conductive 3D framework with a MOF coating to obtain a MOF-coated composite current collector. There are several structural advantages of the obtained composite Li-metal current collector. The lower regions of the porous 3D framework can be used as a storage region for metallic lithium, achieving high area capacity and suppressing dendrite growth. The porous MOF layer on the top can be used as an "ion sieve" as it possesses adjustable pore size, good insulation, and electrochemical stability, in which case, it is conducive to the uniform distribution of lithium ions. Besides these factors, the high Young's modulus ($>$ 32 GPa) of a MOF layer can further inhibit dendritic lithium growth. Thanks to the above-mentioned advantages, the MOF-HCF@Li anode and a high-area LiFePO$_4$ cathode-matched full battery prepared by them achieved a long cycle life of 200 cycles with a high-capacity retention rate of 93%. The schematic diagram of the MOF-HCF current collector is displayed in Figure 5(a).[126] In short, the composite Li-metal anodes prepared in this way show the minimal dimensional change ($<$ 5%), excellent symmetrical battery stability performance ($>$ 1000 h), and full battery ($>$ 200 cycles) performance.

In addition, ZIF-8[128] (classical MOF material), carbonized ZIF-8 material (cMOF),[129] ZIF-67[130] and MOF-199[128] have also been used to uniformly control the deposition behavior of lithium. The porosity and lithiophilic properties of MOFs are important factors helping them serve as a 3D framework to protect lithium anodes. Therefore, lithium anode can be constructed with high ion diffusion and good electron transport dynamics by designing reasonable material compositions and structures.

Recently, Liu et al.[132] achieved dendrite-free and stable Li-metal batteries via a cucumber-like lithiophilic composite skeleton (CLCS). As illustrated in Figure 5(b), a CLCS was fabricated through a unique oxidation-immersion-reduction method with a simple preparation process. Figure 5(c) shows that Li-metal exhibits different deposition and growth behavior on bare metallic copper foam and CLCS. The presence of a large number of pyridinic N, pyrrolic N, and Cu$_x$N sites with excellent lithiophilicity in the structure, which have a high binding energy with lithium ions, can effectively disperse the distribution of lithium ions on the substrate surface and finally achieve uniform lithium deposition as well as inhibiting the development of lithium dendrites. Due to the good suppression of lithium dendrites, this lithium-friendly composite framework can be used for electrochemical performance testing with stable cycling of 700 cycles at 1 mA cm^{-2} and maintain a higher Coulombic performance about 97.3%. The symmetric cell test also maintains a stable cycle life of 2000 hours at 1 mA cm^{-2}.

Batteries & Supercaps

Review
doi.org/10.1002/batt.202200231

Chemistry
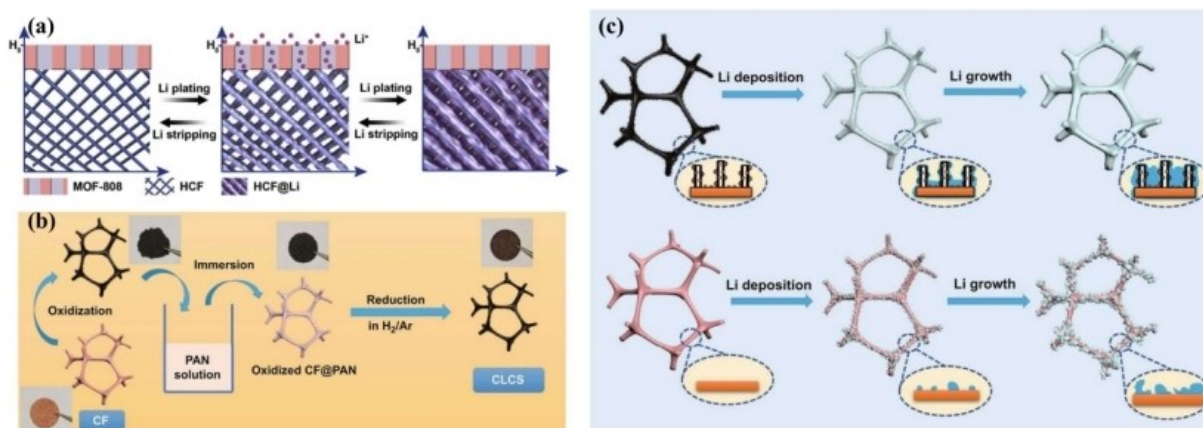Europe
European Chemical
Societies Publishing

Figure 5. a) Schematic diagram of MOF-HCF current collector. Reproduced with permission from Ref. [126]. Copyright (2019) Elsevier. b) Schematic diagram of the synthesis process of CLCs. c) Metal lithium exhibits different deposition and growth behavior on bare metallic copper foam and CLCs. Reproduced with permission from Ref. [132]. Copyright (2021) Springer Nature.

In conclusion, the conductive 3D frameworks change the morphology of the lithium anode from 2D to 3D and have many advantages for dendrite inhibition. We have learned that "Sand's Time" is inversely proportional to the current density (J) based on the Space-Charge Model introduced above. The conductive 3D framework has a high specific surface area due to its 3D network structure, which leads to a significant reduction in the local current density, which delays the "Sand's Time" significantly. Moreover, the conductive 3D framework is more stable, which prevents the infinite volume expansion of lithium and maintains the mechanical stability of the SEI layer.[132] In addition, the functional groups of the 3D framework can promote the uniform distribution and deposition of lithium ions, which fundamentally inhibits the growth of lithium dendrites.

4.2. Optimizing and modifying electrolyte components

Optimizing and modifying electrolyte components facilitates interface engineering, because these can form an enhanced protective film on the surface of the Li-metal anode.[133] Despite the fact that the formation strategy of SEI films is complicated and still controversial, it is generally believed that organic electrolytes usually react with anode materials to form SEI due to their limited electrochemical stability window.[134] Organic electrolytes with additives will generally participate in the formation of shells of solvated lithium ions. In Li-metal batteries, the solvated shell will participate in reactions to form an SEI on the surface of lithium.[135] Therefore, changing the composition concentration and additives of the electrolyte can effectively change the composition of SEI and regulate the deposition behavior of lithium to inhibit dendrite growth.[134–136] Moreover, the improvement strategy for electrolytes can be further applied to high-power Li-metal batteries on a large scale. Therefore, electrolyte optimization (including the optimization of solvents, lithium salts, and the use of additives) is generally reflected to be the furthermost feasible, effective, and

economical method for responding to the demands of new energy storage technologies.[137]

The electrolytes used for Li-metal batteries mainly included solid-state electrolytes and liquid electrolytes. Nearly all the liquid electrolytes react with Li-metals, resulting in low Coulombic efficiency. For instance, ester-based electrolytes are more reactive with Li-metals than ether-based electrolytes, leading to dendritic Li development and poor Coulombic performance.[138] When compared to liquid electrolytes, solid-state electrolytes are more stable to Li-metal, although a few of them might partially react with Li-metal. Minimizing reactions concerning Li-metal and solid-state electrolytes can improve Coulombic efficiency, reduce dead lithium, and inhibit lithium dendrite formation. However, dendrite formation can still be a concern in a cell with solid-state electrolytes.[53] However, due to the particularities of solid-state electrolytes (solid-state electrolytes affect the scope of optimization and modification of the metallic lithium surface), we will discuss solid-state electrolytes separately. This section contains the following information, we will only summarize recent advances related to liquid electrolytes.

4.2.1. Highly concentrated electrolyte

Scientists have found that a significantly greater concentration of lithium salt in the electrolyte can effectively suppress the production of lithium dendrites in Li-metal battery systems.[139] The improvement mechanisms of high-concentration electrolytes with Li-metal anodes mainly come from the following two aspects: i) As salt concentration increases, the viscosity of an electrolyte is enhanced and the influence of convective mass transfer weakens. The liquid mass transfer rate on the surface of the Li-metal anode is uniform. ii) The high concentration of salt decreases the amount of free solvent molecules and reduces the reactivity of the electrolyte with lithium.[140]

At present, the main lithium salt in commercial lithium-ion battery electrolyte systems is LiPF$_6$, and the solvent is a

Batteries & Supercaps

Review
doi.org/10.1002/batt.202200231

Chemistry
Europe
European Chemical
Societies Publishing

carbonate-based system. The lithium salt concentration is generally around 1 mol L^{-1}.[127] This electrolyte system is relatively stable in lithium-ion batteries. Around this concentration, the electrolyte has the best ionic conductivity and liquid fluidity. However, this electrolyte also has few drawbacks. The anions in the LiFP$_6$ lithium salt do not participate in the materialization of a stable LiF layer. The ester solvent system will promote the production of more Li$_2$CO$_3$ on the surface. This makes it easy to produce lithium dendrites, resulting in lower Coulombic efficiency. Therefore, there is a need to further study suitable high-concentration electrolytes to reduce the growth of lithium dendrites. Qian et al.[141] pioneered the use of a 4.0 mol L^{-1} LiFSI/DME high-concentration electrolyte system for Li-metal batteries. Compared with low-concentration electrolytes, the morphology of lithium (deposited on Cu foil) showed a stable and dense deposition layer. In the low-concentration system, the surface of the Cu foil presents elongated dendrites. Furthermore, at a current density of 1 mA cm^{-2}, the high-concentration system's Coulombic efficiency maintained around 99.1% after 1000 cycles. When the high-concentration system electrolyte is used in a Li symmetric battery, it shows excellent cycling stability up to 6,000 cycles at a current density of 10 mA cm^{-2}. Matsumoto et al.[142] recently discovered that a high concentration of lithium bis(trifluoromethanesulfonyl) imide electrolyte can effectively minimize the corrosion of aluminum current collectors due to the limited solubility of Al(TFSI)$_3$.

Highly concentrated lithium salt solutions can also promote the improvement of lithium batteries for extreme environments. The concentrated electrolyte can enhance the stability of the electrolyte with an electrode-interface, but its high viscosity prevents lithium ions from migrating. Recently, Xia et al.[143] designed a co-solvent electrolyte to enable high-energy Li-metal batteries operated at −70 °C. They diluted a concentrated EA (ethyl acetate) based electrolyte with electrochemically "inert" dichloromethane (DCM). The co-solvent electrolyte in this instance had a high ionic conductivity (0.6 mS cm^{-1}) at −70 °C, low viscosity (0.35 Pa s), and a large electrochemical window (0–4.85 V). As a result, they realized a Li-metal battery with an energy density of 178 Wh kg^{-1} and a power density of 2877 W kg^{-1} at −70 °C. Their research has made a landmark contribution to the study of rechargeable lithium-based batteries under extreme conditions. However, the relatively low boiling point of DCM may limit its use at high temperatures. Further research is needed in this regard.

It is well-known that the most widely-used carbonate electrolytes have poor dynamic performance and do not match the thermodynamics of the Li-metal anodes. It is easy for carbonate electrolytes to form a physically and chemically unstable SEI film on the surface of the Li-metal anodes.[144] The corrosion and dendrite formation of Li are accelerated as a result of this. Until now, the charge-discharge Coulombic efficiency of Li-metal with conventional carbonate-based electrolytes has difficulty exceeding 98.5%, especially under high-rate cycling conditions.[145] Meanwhile, nitrile organic solvents are stable as high as ~5 V and can cover the working voltage window of current mainstream battery cathode materials with

a high dielectric constant, low viscosity, and good dissociation effects. These can form electrolyte systems with excellent dynamic performance, which has been widely used in supercapacitors. However, nitrile solvents are highly corrosive to Li-metal and have not been utilized in Li-metal batteries. Recently, Peng et al.[146] developed for the first time a high concentration nitrile electrolyte for high-energy Li-metal batteries. Nitrile solvents are hard to passivate and form films on the surface of Li-metal owning to their distinctive structure, high reduction potential, and a large number of side reactions that continue to occur. Even when using lithium bisfluoro-sulfonimide salt (LiFSI), the concentrated electrolyte with acetonitrile (AN) as the solvent can only reach 10% Coulombic efficiency with Li-metal. Therefore, they proposed to use the fundamental film-forming additive, vinylene carbonate (VC), combined with the strong coordination effect of the lithium salt and the solvent in a high salt concentration system. Meanwhile, they also adjusted the salt concentration to control the reduction of the electrolyte. As a result, an optimized acetonitrile high salt concentration electrolyte system (LiFSI:AN:VC, LAV system) was prepared. A stable SEI film based on cross-linked polycarbonate and lithium fluoride was grown on the surface of Li-metal. This type of high salt concentration electrolyte not only has the high oxidation stability of nitrile solvents but also has a Coulombic efficiency of over 99.2% with Li-metal. In addition, it has excellent high-current performance and can achieve dense Li-metal deposition at a current density of 4 mA cm^{-2}. Exercising this nitrile high-salt electrolyte can realize stable cycling of a 4.5 V Li-metal battery with a higher current density (above 2 mAh cm^{-2}).[146]

Especially given the fact that high-concentration electrolytes have been demonstrated to be able to improve the durability and efficiency of lithium anodes. However, the cost of high-concentration electrolytes is high and the liquid flowability is poor. There is a need to design more economical electrolytes with optimal composition and suitable concentration for lithium metal batteries to reduce overall costs.

4.2.2. SEI stabilizing additives

Adjusting SEI composition by adding a small amount of electrolyte additives is a simple and effective strategy to strengthen SEI films and improve the anode interface to reduce the growth of lithium dendrites. By using additives, the uniformity and stability of the SEI film can also be greatly optimized. Electrolyte additives can decompose, adsorb and polymerize on the surface of Li-metal, so as to enhance the uniformity of SEI film and improve the current distribution on the electrode surface during lithium plating. The enhancement consequence of SEI be influenced by the degradation reaction process of additives and reducing the Li surface. Due to its high activity, metallic lithium reacts with most liquid electrolytes. Choosing film-forming additives is generally needed for optimizing electrolyte composition and Li-metal reactions to form stable compositions at the same time.[126] Therefore, good film-forming additives generally need to have the following

Batteries & Supercaps

Review
doi.org/10.1002/batt.202200231

Chemistry
Europe
European Chemical
Societies Publishing

features: Firstly, additives need to have lower LUMO (Lowest Unoccupied Molecular Orbital) energy levels and higher HOMO (Highest Occupied Molecular Orbital) energy levels to match metallic lithium's energy levels. Secondly, the reaction products of additives, with Li-metal need to maintain good chemical and electrochemical stability and have appropriate electronic insulation and ionic conductivity. In addition, the SEI formed needs to maintain a compact and continuous structure.[127] A high Young's modulus is also crucial to inhibiting the generation of lithium dendrites for Li-metal anodes.[147] LiF has a higher value of Young's modulus (~ 64.9 GPa) and electronic insulation properties (10^{-31} S cm^{-1}), which meet the above requirements well.[148,149] Therefore, choosing appropriate fluorine-containing additives to construct a LiF-rich SEI on the surface of lithium may successfully reduce the growth of lithium dendrites.[127]

At present, a variety of electrolyte additives was utilized to stabilize the SEI of graphite or silicon-based electrodes.[150,151] Many additives have been successfully designed such as FEC (fluoroethylene carbonate),[147–149] VC (ethylene carbonate),[155,156] ES (vinyl sulfite),[157,158] and other emerging additives (including LiNO$_3$ and polysulfides),[159] etc. Apart from these, there are still a large number of element additive systems containing F, N, S, and B used to stabilize SEI, such as LiAsF$_6$,[160] LiBOB (lithium dioxalate borate),[161] LiDFOB (Lithium difluoroxalate borate),[162] LiPS (Lithium polysulfide),[163] H$_3$BO$_3$,[164] etc.

As is well known, the traditional LiPF$_6$ electrolyte (one of the most successful lithium salts in commercialization) forms poor SEI, which contains a large amount of LiF and Li$_2$CO$_3$ resistive decomposition products and other inorganic and organic by-products. Zheng et al.[165] found that the optimal amount of LiPF$_6$ (0.05 M) as an electrolyte additive for LiTFSI-LiBOB dual-salt/carbonate solvent can remarkably enhance the cycling stability and specific capacity and of Li-metal batteries. To decrease the formation of high-resistance LiF, the content of LiPF$_6$ additives in the dual-salt electrolyte is very important. Zheng et al.[165] found that under the condition of 1.75 mA cm^{-2}, adding 0.02 M LiPF$_6$ can greatly increase the cycle life of Li$\|$NMC batteries. When the concentration of LiPF$_6$ is increased to 0.05 M, the cycling stability of the battery reaches its maximum. When the LiPF$_6$ content was further increased to 0.1 M and 0.2 M, the battery performance (including stability and battery capacity) was noticeably decreased. The reason is that too much LiPF$_6$ additive (0.1 M and 0.2 M) makes the dual-salt electrolyte behave more like a pure LiPF$_6$-based electrolyte. In other words, more LiPF$_6$ will dominate the formation of SEI and accelerate the consumption of electrolytes, similar to traditional LiPF$_6$/carbonate electrolytes. When the amount of LiPF$_6$ is 0.05 M, the Li-metal battery with 4 V lithium-ion cathode can maintain 97.1% capacity to beyond 500 charge/discharge cycles under a medium-high load condition of 1.75 mAh cm^{-2}. At the same time, the increase in the electrode over potential remains mild. The main reason for fast charging and stable cycling is the formation of a solid and conductive electrolyte mesophase on the surface of Li-metal, which stabilizes the aluminum collector. The LiPF$_6$ additive is important for stabilizing the Al current collector. Moreover, it also induces the production of a strong conductive SEI layer rich in polycarbon-

ate. The SEI can promptly and efficiently separate any "dead" Li and the bulk Li metal anode. The promoted interface stability enables Li metal batteries to operate continuously at high current density.[165] These key findings provide insights that can be used to stimulate revolutionary improvements in Li metal batteries' performance by manipulating the salts, solvents, and additives of electrolytes.

Li et al.[166] suggested a simple as well as efficient interface in-situ catalytic grafting technique to obtain Li-metal anodes with maximum reliability, excellent stability, and dendrite inhibition, given the poor flexibility of inorganic components of the SEI layer and the complicated phases, morphologies, and reaction mechanisms of the existing organic-inorganic hybrid SEI layers. The researchers employed a graftable additive, liquid polydimethylsiloxane concluded with a —OCH$_3$ group (PDMS-OCH$_3$), to induce "grafting" on the surface of Li-metal using the electrochemical electric field and electric potential. Figure 6(a) shows in situ grafting of PDMS-OCH$_3$ on LiOH and Li$_2$O thin skins on the Li anode. The thin "skin" of Li$_2$O and LiOH normally observed on the surface of Li-metals may activate and catalyze the dissolution reaction of PDMS-OCH$_3$ during charge transfer activity, as shown. Smaller molecules can really be polymerized into inorganic Li$_x$SiO$_y$ fast ion conductors by grafting broken macromolecules onto to the surface of Li-metal. The large proportion of LiF introduced during the electrochemical reaction enhances such an organic-inorganic hybrid interfaces phase (i.e., grafted SEI). The integration of Li$_x$SiO$_y$ and LiF hard inorganic components can produce fast ion diffusion channels and interfaces, accomplishing the ion flux homogenization effect. And it can act as a barrier to the growth of lithium dendrites. The soft PDMS branches may increase elasticity and buffer the entire SEI effect. As represented in Figure 6(b), Li/Li symmetric cells using PDMS addition perform better on Li plating-stripping than those without PDMS addition. Moreover, the insets of Figure 6(b) shows that even after a long period of cycling, the voltage profile shows a clear plateau region. This indicates that the PDMS grafted layer actually plays a significant part in promoting the growth of high reversibility and stability modulated of Li nucleation. Liquid PDMS additives have even more substantial advantages in terms of Li-metal densification and SEI stability than solid siloxane additives having poor grafting potential (such as polyhedral oligomeric silsesquioxane (POSS) ended by eight phenyl-groups). There is a benefit from the liquid state and linear structure of PDMS additive. Comparison of the molecular structures of linear PDMS and caged POSS is shown in Figure 6(c and d). The linear structure of PMDS results in a large contact area on Li surface, this causes it to "graft" on Li anode, whereas POSS' cage-like structure with relatively inert terminal groups makes it difficult to produce grafts. As a result of this, Li/Li symmetric cells with 8% PDMS additive altered systems perform better in Li plating/stripping than cells with 0.1 wt% POSS additive modified systems.[166]

In addition, studies have also explored lithium polysulfide compounds and LiNO$_3$ added to ether electrolytes, in which case, the uniformity of lithium plating can be significantly improved. The generation of lithium dendrites can be con-
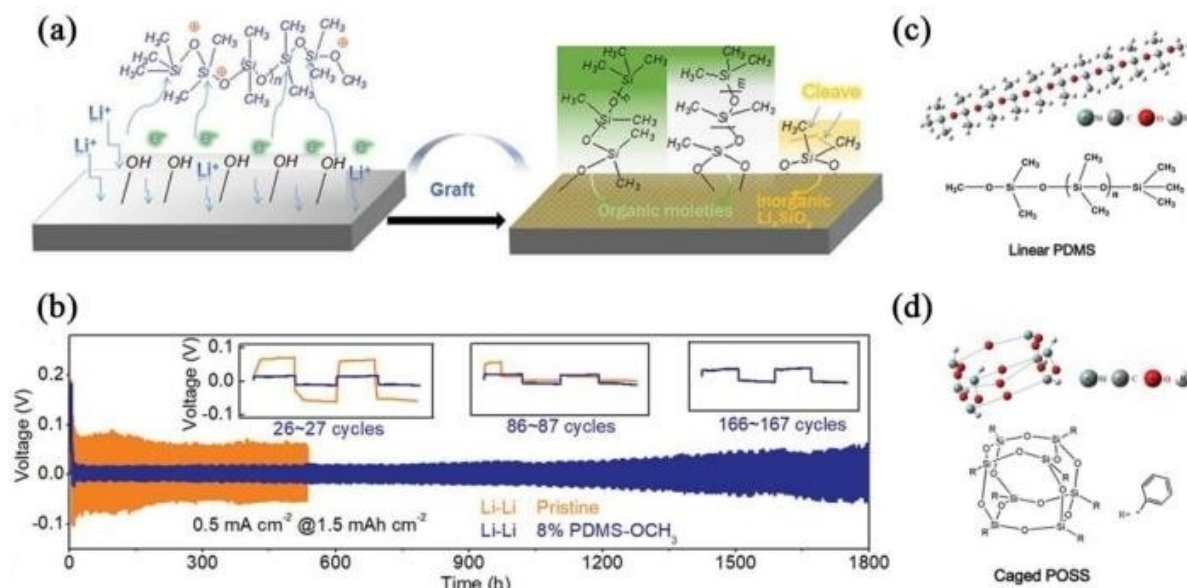
Batteries & Supercaps

Review
doi.org/10.1002/batt.202200231

Chemistry Europe
European Chemical
Societies Publishing

Figure 6. a) Schematic of in situ grafting of PDMS-OCH$_3$ on thin skins of LiOH and Li$_2$O on Li anode as well as the Lithium deposition in electrolytes with and without PDMS addition. b) Li plating-stripping performance comparison of Li/Li symmetric cells with and without PDMS addition. Insets: corresponding voltage profiles at different cycling stages. c) Molecular structures and formula of PDMS terminated by —OCH$_3$ group and d) POSS terminated by —C$_6$H$_5$ groups. Reproduced with permission from Ref. [166]. Copyright (2019) WILEY-VCH.

trolled, and the cyclic performance of the resultant battery can be enhanced. Therefore, LiNO$_3$ is often used in lithium-sulfur batteries to inhibit the formation of lithium dendrites. The mechanism underlying this method forms a passivation layer via the reaction of LiNO$_3$, and metallic lithium and then lithium polysulfide compounds react with the passivation layer to form Li$_2$S and Li$_2$S$_2$.[23] LiNO$_3$ effectively inhibits the formation of CH$_4$ and H$_2$ and promotes the generation of N$_2$ and N$_2$O. These gases help repair the SEI film and stabilize the entire battery system. Moreover, near the end of the charging process, nitrate ions (NO$_3^-$) can accelerate the conversion of polysulfides to elemental sulphur. The strong "bond-like" effect between nitrate ions (NO$_3^-$) and polysulfides inhibits the diffusion of sulfide. A homogenous and stable SEI layer could be created on the surface of the anode by regulating the concentration of polysulfide and LiNO$_3^-$ in ether-based electrolytes, which potentially reduces the decomposition of the electrolyte.[167] The types of polysulfide present will also disturb the performance and composition of the formed SEI film. Studies have shown that polysulfides with longer chain lengths, especially Li$_2$S$_5$, are the most promising polysulfide additives to form an effective SEI layer.[168] In addition, the amount of polysulfide added also has an important influence. Therefore, the selection of polysulfides and the optimal ratio of polysulfides to LiNO$_3$ need to be determined by specific analysis. In addition to polysulfide additives, researchers have also developed sulfur-containing polymers as electrolyte additives such as poly(sulfur-random-triallylamine) (PST)[169] and poly (sulfur-random-1,3-diisopropenylbenzene).[170]

In addition to these industrial-style additives, recently, Wang et al.,[171] inspired by the natural biological immune mechanisms, discovered a protein additive that can signifi-

cantly decrease the growth of dendrites of Li-metal anodes. The protective mechanism of the protein on the surface of metallic lithium is demonstrated in Figure 7(a). Firstly, due to the structural characteristics of the protein itself and the denser charge distribution at defects and sharp tips, this protein could be adsorbed more effectively here on the surface of Li-metal anodes with a smaller curvature (such as edges, corners, dendrite tips, and other defects). After being in contact with the surface of the Li-metal anodes, its unique hydrophilic/hydrophobic interface can induce the transformation of the secondary structure of the protein molecule (from α-helix to β-Sheet), which strengthens the adsorption of the protein on the surface of Li-metal. When the protein molecules are attached to high surface area tips, the electric field intensity near those tips is greatly reduced, which induces the subsequent lithium ions to diffuse to the surrounding area and deposit away from the tips, in which case, the rapid generation of lithium dendrites can be effectively avoided. In addition, part of the protein adsorbed on the surface of the Li-metal will be reduced through the Li-metal during the process of deposition and contribute to the formation of the SEI. Observations by cryo-electron microscopy show that the thickness of the SEI with protein participation is much greater compared to SEI designed in the pristine electrolyte. The X-ray depth component analysis results show that the SEI with proteins involved in the formation has a higher Li$_3$N composition, which is dominated by c-Li$_3$N. The changes in the composition of the SEI improve its mechanical properties and enhance the permanence of the Li-metal surface. In short, protein dispersed in electrolytes can be selectively adsorbed, which can change the distribution of the electric field on the surface of the Li-metal anodes and directly take part in the growth process of the SEI film, thereby
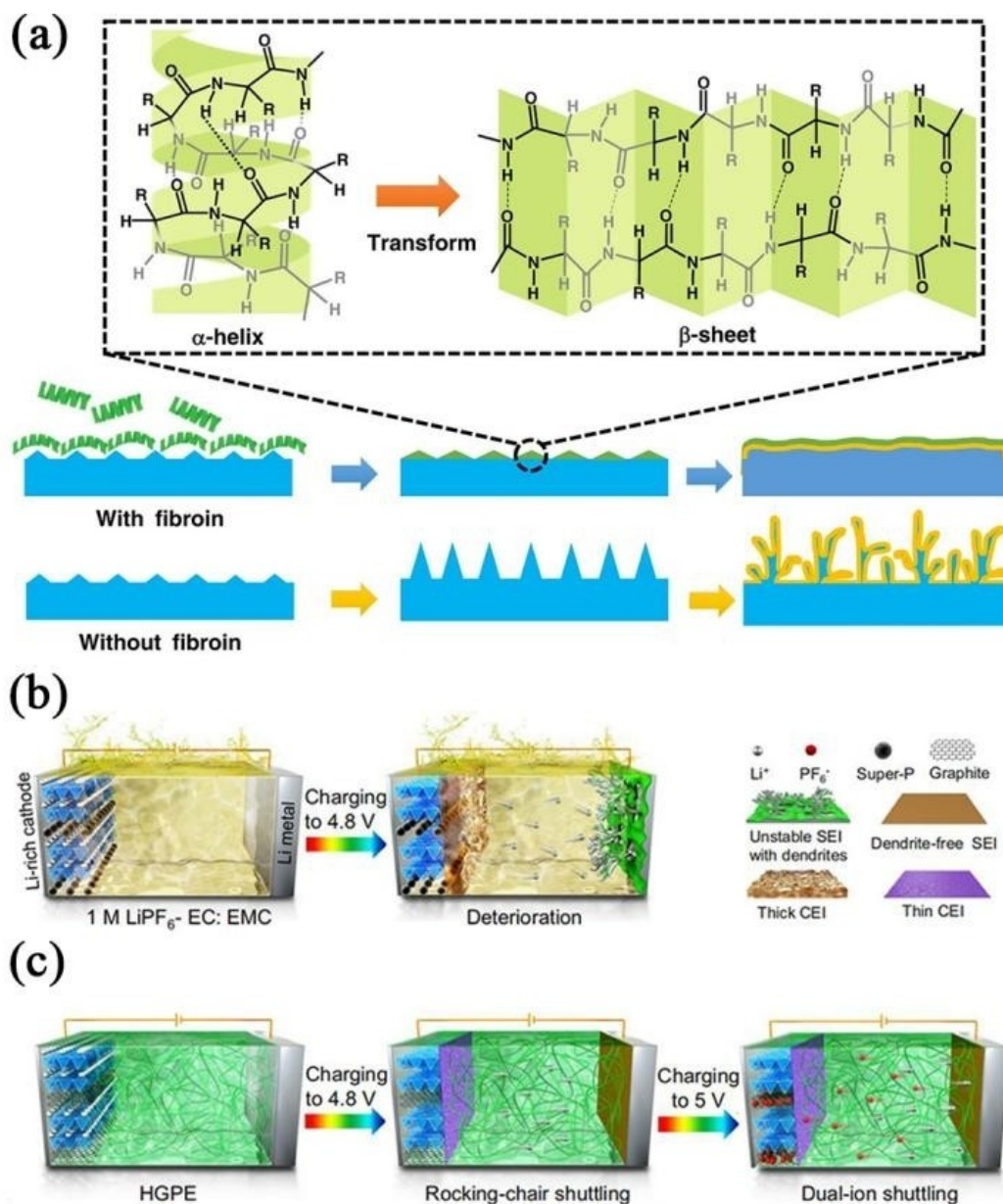
Figure 7. a) Schematic diagram of the protective mechanism of proteins on the surface of Li-metal and the secondary structure transformation of protein molecules after interacting with the surface of Li-metal. Reproduced with permission from Ref. [171]. Copyright (2020) The Authors. b) Schematic illustration of the mechanisms of a Li|1 M LiPF6-EC: EMC|LRO0 "rocking-chair" battery. c) Schematic illustration of the mechanisms of a "shuttle-relay" battery with a hybrid LRO cathode using graphite as a conductive agent, a Li metal anode, and an HGPE. Reproduced with permission from Ref. [172]. Copyright (2021) The Authors.

promoting the uniform deposition of Li-metal. This ultimately achieves the purpose of eliminating the generation of lithium dendrites, extending the cycle life of the Li-metal anodes, and improving Coulombic efficiency. Wang et al. also proposed a slow-release approach to overcome the reduced dispersibility of proteins in ether-based electrolytes, resulting in a considerable increase in Li-metal battery cycling stability(more than 2000 cycles). This work reveals that the properties of biological macromolecules like proteins can successfully prevent the generation of lithium dendrites, thereby providing the feasi-

bility for realizing stable and safe higher-energy-density Li-metal batteries.[171]

Wu et al.[172] reported a heteroatom-based gel polymer electrolyte (HGPE), which promotes development of high-voltage solid Li-metal batteries. The HGPE was obtained by adding diethyl allyl phosphate (DAP) monomer into an all-flfluorinated electrolyte (contains $LiPF_6$, flfluoroethylene carbonate (FEC), 2,2,2-triflfluoroethylmethyl carbonate (FEMC), 1,1,2,3,3,3-hexaflfluoropropyl-2,2,2-triflfluoroethylether (HTE)). The electrolyte has a high level of safety (leakage and nonflammability), a high level of ionic conductivity

Batteries & Supercaps

Review
doi.org/10.1002/batt.202200231

Chemistry
Europe
European Chemical
Societies Publishing

(1.99 mS cm^{-1} at 25 °C), and a wide electrochemical window (up to 5.5 V vs. Li/Li$^+$), as well as integration including both Li metal anodes (a Li stripping/deposition Coulombic efficiency of 99.7%) and graphite cathodes (93% capacity retention after 1000 cycles). On this basis, Wu et al.[172] created an SRLMB ("shuttle-relay" Li metal battery) with a hybrid cathode containing Li-rich oxide (LRO) as the active material, KS6 graphite as a conductive agent, and HGPE as the electrolyte. Due to the stable electrode interface, SRLMB exhibits high capacity and cycle stability. Figure 7(b and c) depicts the quasi-solid-state SRLMB's operating mechanism, which is realized through a well-designed HGPE. Figure 7(b) shows the working mechanism of a conventional lithium-ion battery. Figure 7(b) shows that the electrolyte solvents cannot create a sustainable SEI layer on the Li metal surface on the anode side. Carbonate solvents with insufficient oxidation resistance cause significant electrolyte breakdown, and on the cathode side, this has a significant impact on battery performance. FEC, DAP, FEMC, and HTE binding energies for a Li$^+$ cation and a PF$_6^-$ anion were compared, including both Li$^+$ and PF$_6^-$, the HTE has the lowest absolute values of binding energy, reflecting a poor interaction between ions and HTE. Therefore, the battery performance can be improved by introducing HTE to obtain a concentrated electrolyte in a local region. When used in SRLMBs, the HGPE provides a unique mechanism (the shuttle-relay shuttle relay) that utilizes the rocking-chair function of LRO with the dual-ion dynamics of graphite in a synergistic manner. As shown in Figure 7(c), in HGPE, the fluoride solvent component in the electrolyte effectively increases the oxidative stability of the electrolyte while constructing a robust SEI/CEI film with synergistic effects of phosphorus-containing monomers, increasing the compatibility of the electrode. Further, the polymer matrix effectively prevents the transfer of Li$^+$/PF$_6^-$ ions from the surface defects of CEI/SEI through a deep interaction, thereby facilitating uniform deposition or embedding of Li$^+$/PF$_6^-$ ion.[172] The results by Wu et al.[173] have shown that lithium-lithium symmetric batteries with HGPE exhibit smaller, more stable polarized voltages and longer cycle life. The metal lithium deposited in HGPE is dense and uniform, effectively inhibiting the formation of lithium dendrites. This dense lithium deposition successfully reduces the parasitic reaction concerning metal lithium and electrolytes. This superior cycle stability is generally due to HGPE efficiently preventing the solvent from degrading the structure integrity, thereby allowing the anions to reversely insert or migrate out of the KS6 graphite. Their research has unlocked novel ways for the development of Li-metal batteries with high energy density for next-generation next-generation high-energy-density.

Electrolyte additives are extremely significant for studying the protection and stability of Li-metal anodes. Further in-depth studies should be continued to achieve better performance of Li-metal batteries. In this case, an SEI film having higher compactness and ionic conductivity may be formed to constrain the development of lithium dendrites. However, there are a few obstacles to the development of electrolyte additives.[174] Firstly, the cost of electrolyte additives is relatively high, which hinders their commercialization.[175] Secondly, most

of the reports showed that the durability of the electrolyte additives is also mediocre, as they will be consumed during cycling and cannot support a sustainable role in long-term cycling. It is believed that by solving these obstacles, lithium metal batteries will become closer to practical applications.[176]

4.3. All-solid-state lithium metal batteries (ASSLMBs)

The organic solvent electrolytes applied in traditional lithium secondary batteries are one of the major reasons causing battery safety problems. When organic electrolytes are replaced with non-flammable solid-state electrolytes, potential battery safety hazards can be effectively eliminated. Therefore, the application of all-solid-state Lithium metal batteries (ASSLMBs) which using solid electrolytes as well as Li-metal anodes can both solve the safety hazards and increase the energy density of the batteries. To enable solid-state electrolytes to be used in practical Li metal batteries, several criteria need to be met.[23] First of all, a high strength modulus is essential, to prevent Li dendrites from penetrating. Secondly, sufficient lithium-ion conductivity is also needed at ambient temperature. Moreover, a wide electrochemical stability window without cathode or anode material decomposition is necessary. And lastly, effective solid-state electrolytes need low interfacial resistance and good adhesion to the electrodes.[177] Versatile processing, low flammability, strong mechanical resistance, and good electrode/electrolyte interface qualities make polymer electrolytes good electrode/electrolyte interface materials.[178]

Solid-state electrolytes that meet the requirements can be broadly classified into two categories, including inorganic ceramic electrolytes (ICEs) and solid polymer electrolytes (SPEs).[179] There are currently two main types of SPEs: all-solid-state single-ion conducting polymer electrolytes (SIPEs) and cross-linked gel polymer electrolytes (CGPEs). Among them, with the presence of organic solvents as plasticizers, CGPEs have excellent ionic conductivity (greater than 10^{-4} S cm^{-1}) and improved electrolyte/electrode interface characteristics properties. The cross-linked structure can promote relatively uniform Li$^+$ flux and accommodates volume change during Li deposition, thereby preventing dendrite growth. However, CGPEs must make a balance between their electronic conductivity and mechanical strength. The weak interaction between the polymer matrix and the intermediate products of conversion batteries is not enough to inhibit unwanted shuttling.[180] Therefore, it is still an urgent mission to develop a polymer electrolyte suitable for conversion-type Li-metal batteries. Wang et al.[181] realized a stable quasi-solid Li metal battery using a layered multifunctional polymer electrolyte (HMPE). They polymerized lithium [1-[3-(methacryloxy) propanesulfonyl]-1-(trifluoromethanesulfonyl) imide (LiMTFSI) and pentaery-thritol tetraacrylic acid in situ in a traditional liquid electrolyte ester (PETEA) monomer to prepare the mixed electrolyte, which is then absorbed by a glass fiber membrane coated with a polymer (3,3-lithium dimethacrylate) (PDAALi). This well-designed HMPE also has high ionic conductivity (2.24× 10^{-3} S cm^{-1}), near-single ionic conductivity (the migration

Batteries & Supercaps

Review
doi.org/10.1002/batt.202200231

Chemistry Europe
European Chemical
Societies Publishing

number of Li-ion is 0.75), good mechanical strength, and significant inhibition of dendrites.

The above section introduced the strategies focusing on SPEs, but combining the advantages of each material may be the optimal solution. SPEs generally have good flexibility and low contact resistance with electrode materials, but they have low strength and can be broken by lithium dendrites. ICEs generally exhibit satisfactory ionic conductivity and mechanical characteristics.[182] The endless development of lithium dendrites can be prevented. However, with poor adhesion of ICEs,[183] electrochemical stability will be less satisfactory.[184] Cyclic voltammetry redox reactions could not be observed at the electrode/electrolyte interface, suggesting the generation of an ion barrier may seriously affect cell kinetics. Therefore, the composite of high conductivity inorganic ceramics and soft polymer electrolytes could provide an ideal solution for high-performance solid-state electrolytes. The composite material can arrange 1D or 2D inorganic materials vertically in the polymer matrix, which provides high mechanical strength and efficient vertical transport of lithium ions and improves flexibility. The interface engineering among electrode and solid-state electrolyte is the key to improving the adhesion performance of electrolyte and extending the electrochemical stability window.[9] Recently, Aetukuri et al.[185] developed a membrane that combines one-particle-thick $Li_{1.6}A_{0.5}Ti_{0.95}Ta_{0.5}(PO_4)_3$ with a flexible polymer. The membrane can provide both flexibility and dendrite suppression. A polymer/ceramic/polymer sandwich structure is proposed.[186] $Li_{1.3}Al_{0.3}Ti_{1.7}(PO_4)_3$ (LATP) was compounded with crosslinked poly (ethylene glycol methyl ether acrylate) to obtain a soft interface to a ceramic body with mechanical strength, which solved the problems of elastic modulus adhesion and Li dendrite development. Yu et al.[187] used poly(ethylene oxide) (PEO) with succinonitrile (SN) and oxidation-resistant poly(acrylonitrile) (PAN) substrate mixed with lithium aluminum titanium phosphate ($Li_{1+x}Al_xTi_{2-x}(PO_4)_3$, LATP) as a multi-layer laminated dual-polymer/polymer-ceramic composite electrolyte (LDPPCCE) for high-voltage all-solid-state lithium metal batteries. The anode-friendly PEO has improved room temperature ionic conductivity due to the addition of SN. The PEO-SN-LiTFSI dual polymer layer with anti-reduction function ensures the electrochemical stability of the lithium metal anode. On the other hand, the addition of LATP on the cathode side enhances the ionic conductivity of PAN and also inhibits the growth of lithium dendrites, thus the PAN-LATP-LiTFSI makes it possible to use high capacity and high voltage cathodes. In addition, the PEO-SN-LiTFSI dual polymer avoids the incompatibility problem between lithium metal and LATP or between lithium metal and PAN. The ionic conductivity of the as-prepared electrolytes is up to 1.31×10^{-4} S cm^{-1} with an electrochemical stability window of 0–5 V. For full cell testing with the lithium metal anode and $LiNi_{0.8}Co_{0.1}Mn_{0.1}O_2$ cathode, a stable Coulombic efficiency of around 98.8% can be maintained up to 300 cycles.

However, the contact resistance among metallic lithium and the solid-state electrolyte is also relatively large, and lithium dendrites can be generated during cycling. When the current density is large, the high interface contact resistance will seriously increase the polarization of the battery. To solve this problem, Duan et al.[188] blended an appropriate amount of graphite additives into molten lithium to develop a Li-C composite. The molten Li-C composite shows low fluidity and high viscosity than pristine lithium. The molten Li-C anode is coated on pomegranate-type inorganic ceramic solid-state electrolyte $Li_{6.5}La_3Zr_{1.5}Ta_{0.5}O_{12}$ (LLZTO) to construct a uniform and stable Li-C/LLZTO interface. Duan et al.'s study has shown that LLZO has better compatibility with Li-C composites. The molten Li-C composites can be adsorbed on the surface of LLZTO very well, while molten Li is not spontaneously absorbed on LLZTO. Duan et al. also found that the Li-C electrode and LLZTO electrolyte are in close contact, and the interface impedance is 11 Ω cm^{-2}, while there are several micron gaps between the Li electrode and LLZTO, and the interface impedance is higher about 381 Ω cm^{-2}. Thanks to the stable interface, the Li-C/LLZTO/Li-C symmetric battery can be cycled stably for 250 h at a current density of 0.3 mA cm^{-2}. When Li-C/LLZTO and LFP compose a full battery, it can cycle stably for 100 cycles at a current density of 0.5 C as in older-style liquid electrolyte systems. By comparison, when a pure Li-metal anode is used (i.e., no C), the battery capacity quickly decays to zero.[188]

In short, solid-state electrolyte modified layers avoid the influence of convective mass transfer on the lithium-ion transmission rate and homogenize the mass transfer flow of lithium ions on the surface of the anodes.[189] In theory, this is an encouraging process for improving the rechargeability of Li-metal anodes.[190] However, in the actual system, it is hard to form and maintain a uniform contact interface between Li-metal anodes and solid-state electrolyte, and it is difficult to maintain the uniformity of the solid-state electrolyte and the conductivity of different microdomains. These factors cause uneven distributions of current density on the surface of the Li-metal anodes and promote dendrite growth.[191] Solid-state electrolytes are also relatively thick (>100 μm) and small in area (<5 cm^2) on inorganic ceramics. There is a need to further develop economical methods to make solid-state electrolytes that are thinner yet larger in area for practical applications.

4.4. Artificial SEI improves Li-metal anode

As mentioned above, unstable SEI films adversely alter the electrochemical efficiency and cycle life of Li-metal anodes. Uneven distribution of electric field, rough surfaces and nonuniform flux of lithium ions are major factors to accelerate dendrite formation. Furthermore, any growth of lithium dendrites will further destroy the SEI structure and eventually cause safety issues.[190–194] Therefore, SEI thin films are very important for outstanding long cycle life and energy storage performance. Currently, the commonly used method for optimizing SEI is to design a protective film as an artificial SEI.[195–197]

The current artificial SEI can be realized by a variety of methods such as gas-solid reaction formation and liquid-solid reaction formation. The main reason for the popularity of gas-

Batteries & Supercaps

Review
doi.org/10.1002/batt.202200231

Chemistry
Europe
European Chemical
Societies Publishing

phase reagents is that gas-phase reagents have excellent permeability and high accessibility, which allows the establishment of a highly uniform coating on the anode surface. Generally, the formation of an artificial SEI layer can be well controlled by adjusting gas concentration, reaction pressure, temperature and time.[198] Compared with a gas-solid reaction, the reaction occurring at a liquid-solid interface is easier to control and realize. The requirements of the device are easier to meet as the film formation speed changes. Either way has its own unique advantages. The following section describes in detail several artificial SEI films.[147]

It can be seen from the foregoing that LiF can passivate an SEI film as well as limit the growing lithium dendrites owing to its relatively high Young's modulus and electronic insulation properties. Considering the high toxicity of F_2, Cui, et al.[190] used the non-toxic CYTOP amorphous fluoropolymer and commercial Freon R134a as precursors to produce pure F_2 at relatively low temperatures. Then, F_2 reacts with Li-metal to form a compact and uniform LiF coating, thereby effectively protecting the Li-metal anodes. Zhao et al.[199] used a gas-solid reaction to produce an artificial LiF SEI film, which has attracted wide attention due to its large-scale preparation. The preparation process is shown in Figure 8(a). As shown in Figure 8(b), they heated the fluorine-containing organic CYTOP at 350 °C to generate fluorine gas (F_2), and then F_2 reacted with Li-metal for 12 hours to induce a protecting layer of LiF ($\sim$380 nm thickness) on the lithium surface. The symmetrical battery composed of the lithium anode protected by the LiF can be cycled stably for 300 cycles with the following specifications such as depleting capacity of $1\ mAh\,cm^{-2}$ and a current density $1\ mA\,cm^{-2}$. The lithium anode remains stable after cycling

without obvious dendrite formation. Recently, Yan et al.[200] constructed a new type of artificial SEI. They used a displacement reaction to form a composite mixed ionic/electronic conductor interphase (referred to as MCI) on the surface of a Li-metal anode. They used CuF_2 and F_2 to undergo a controlled displacement reaction ($CuF_2 + 2Li \rightarrow 2LiF + Cu$) to form a LIF/Cu protective film (MCI). The displacement reaction makes the rough surface of the Li-metal anode become smooth, which promotes the uniformity of Li-ion flux. The MCI film they designed effectively improves the Li-metal anode, reduces the resistance of the battery, endows the battery with high ion conductivity also, and extends the battery cycle time. Considering the effectiveness of LiF, many research teams have achieved good results using other fluorine-containing compounds to construct SEI films accommodating LiF, such as ZnF_2,[201] AlF_3,[202] NiF_2,[203] SbF_3,[204] $BF_3 \cdot H_2O$[205] and others.

There are many examples of other inorganic materials exercised used to fabricate artificial SEI. The Li_2S shielding layer has been proven to be a stable SEI layer that inhibits the growth of Li dendrites due to its higher ionic conductivity ($\sim$ $10^{-5}\ S\,cm^{-1}$).[206] Li_2Se and Li_2S have similar chemical characteristics and high Li^+ transfer ability. Yu et al.[207] prepared an integrated lithium ion conductive Li_2S/Li_2Se (LSSe) layer with a simple and cheap gas-solid reaction at low temperature. Stable artificial SEI with high ion conductivity was obtained by this technology. The Li|Li symmetrical battery composed of LSSe-protected Li-metal anode (LSSe@Li) avoided all dendritic deposition/exfoliation for more than 900 h under the conditions of $1.5\ mA\,cm^{-2}$ and $3\ mAh\,cm^{-2}$. The fabrication process of LSSe@Li anode is shown in Figure 8(c).
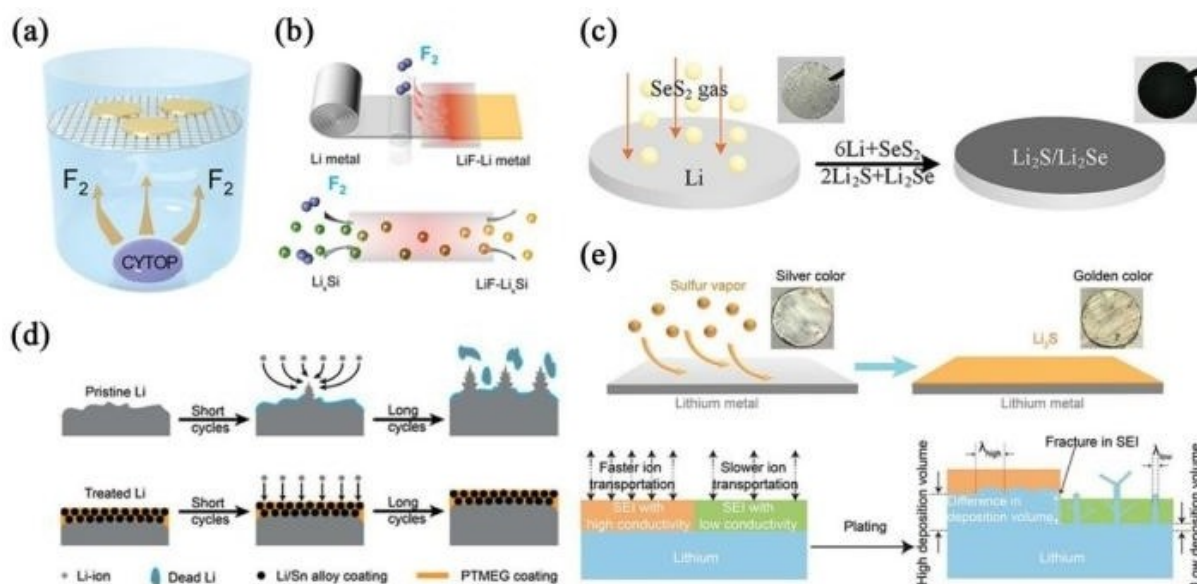

Figure 8. a) Schematic of fabricating LiF protection layer. b) A schematic illustrates that the fluoropolymer, CYTOP, gradually decomposes and releases pure F_2 gas upon heating, which reacts with Li metal or Li_xSi NPs to form a uniform and compact LiF coating. Reproduced with permission from Ref. [199]. Copyright (2017) American Chemical Society. c) Schematic illustration of fabrication process of LSSe@Li anode. Reproduced with permission from Ref. [207]. Copyright (2020) Wiley-VCH. d) Deposition of pristine Li and treated Li. Reproduced with permission from Ref. [215]. Copyright (2019) Wiley-VCH. e) Schematic of the fabrication process and effect of Li_2S protection layer. Reproduced with permission from Ref. [219]. Copyright (2019) Wiley-VCH.

Batteries & Supercaps

Review
doi.org/10.1002/batt.202200231

Chemistry Europe
European Chemical
Societies Publishing

In addition to the inorganic protective layers, many organic polymers such as PVDF-HFP (polyvinylidene fluoride-hexafluoropropylene),[208] high polarization-PVDF,[209] PDMS (polydimethylsiloxane),[210] PEO (polyethylene oxide)[211] and organic (poly) sulfide[212,213] have also used in research on artificial SEIs due to their high toughness and mechanical stability. Polyacrylic acid (PAA) is a typical polymer material used for artificial SEI.[214] This material has strong adhesion and the ability to form a uniform lithium-ion conductive coating. LiPAA polymer is a protective layer obtained by a redox reaction between PAA and lithium. Its simple manufacturing method used also brings convenience and the SEI layer of the LiPAA can automatically adjust mechanical stress, suppress uneven Li plating, reduce side reactions, and achieve stable Li peeling/plating.

When the ionic conductivity of a pure organic polymer system cannot be further improved, it is necessary to combine the advantages of inorganic substances and organic polymers to prepare an artificial SEI layer with higher ionic conductivity and high toughness. Jiang et al.[215] exercised a facile chemical treatment to form a polymer-alloy mixed layer (denoted as treated Li) in situ on the surface of lithium foil. Due to the presence of the alloy, the mixed layer has excellent lithium-ion transport properties, and can uniformly deposit lithium and limit the outgrowth of lithium dendrites. Deposition of pristine Li and treated Li is shown in Figure 8(d). More importantly, due to the hydrophobic nature of the polymer formed in situ, the processed lithium foil can be stably stored in humid air and still retains certain electrochemical activity. From the foregoing, the design of the current collector structure can significantly alleviate the volume expansion of lithium. The electrolyte regulation generates a unique SEI film on the surface of the lithium. The introduction of lithiophilic materials facilitates uniform lithium deposition, and the construction of an artificial protective film can reduce the occurrence of side reactions. However, these studies are focusing on improving the cycle life of Li-metal batteries. Meanwhile, the challenges for large-scale production should also be noted. As is well-known, lithium oxidizes exothermically when reacting with air, especially humid air, which places strict requirements on the large-scale packaging of batteries. Although there have been reports of improving the air stability of Li-metal through atomic layer deposition (ALD) or molecular deposition (MLD) methods, it is still difficult to apply these technologies on a commercial level owing to their complexity and their higher cost. Research by Jiang et al.[215] has made very important progress in this regard. They used a simple and low-cost chemical treatment method by soaking a piece of lithium foil in 0.1 M $SnCl_4$ tetrahydrofuran solution and then added a small amount of propylene oxide to promote polymerization. By doing this, a layer of PTMEG-Li/Sn is formed in situ on the surface of the lithium. This polymer-alloy protective layer has the characteristics of both alloy and polymer. On the one hand, Li/Sn alloy has excellent lithium-ion transport properties, which can uniformly deposit lithium and prevent the growth of lithium dendrites. On the other hand, due to the hydrophobic nature of PTMEG, the processed lithium tablets can be stored stably even in humid air. This

research is of absolute importance to the large-scale application of Li-metal anodes in the future. Besides, this idea can not only be used for Li-metal anode protection but also for the protection of other metal anodes (such as Na, Zn) and the pre-lithiation process of graphite/silicon-carbon anodes. Other hybrid protective layers for artificial SEI include PEO/TiO_2,[216] PMMA (polymethylmethacrylate)/SiO_2[217] and PEDOT-co-PEG (poly3,4-ethylenedioxy-thiophene monomer-polyethylene glycol)/AlF_3.[218]

At present, research on SEI mainly focuses on the use of electrolyte additives, but the SEI obtained by this method is generally a mixture of parasitic products embedded in artificial SEI. The impact on the stability of SEI is rarely reported. The influence of the properties of different SEIs (such as ionic conductivity) on the stability of Li-metal anodes needs to be clarified urgently with the advent of various artificial SEIs (such as LiF, Li_3N, Li_2S, and derivatives). Recently, Cui et al.[219] successfully designed and manufactured a new type of uniform and highly ionically conductive SEI (lithium sulfide). They stabilized Li-metal anodes through a gas-solid interface reaction between sulfur vapor and Li-metal. The fabrication procedure and outcome of the Li_2S protection layer are shown in Figure 8(e). Compared with the traditional electrolyte additive, this artificial SEI with higher ionic conductivity (10^{-5} S cm^{-1}) effectively avoids the introduction of electrolyte by-products with lower ionic conductivity (like lithium fluoride 10^{-9} S cm^{-1} and lithium carbonate 10^{-8} S cm^{-1}), and can be used in traditional carbonate electrolyte systems with low solubility of sulfur additives. At high area capacity and high current density (5 mAh cm^{-2}, 2 mA cm^{-2}), the SEI protective film can still successfully constrain the development of lithium dendrites and achieved 900 cycles stably in a Li-$Li_4Ti_5O_{16}$ full battery. Additionally, Cui et al.[219] conducted XPS analysis, in-situ optical microscopy, and COMSOL simulation. They demonstrated that reducing the complexity of the chemical configuration of the SEI and improving the ionic conductivity of SEI are critical to achieving a stable SEI. In lithium deposition processes, the surface of metallic lithium protected by an SEI with high ionic conductivity easily forms large-size deposits, which is beneficial to the stability of the SEI. In contrast, a surface of metallic lithium protected by an SEI with low ionic conductivity easily forms dendrite-like small particles, which could cause the breakage of the SEI. When SEI from both high and low ionic conductivity exists on the surface of metallic lithium, the metallic lithium is more likely to be deposited on the electrode surface underneath the high ionic conductivity SEI. This leads to uneven deposition volume distribution, which in turn tears the SEI.

As is well known, there are three major problems in the stripping/plating process of Li-metal anodes. One of them is the dendrite growth. The second issue is high chemical reactivity. The third challenge is huge volume changes during plating/stripping. Although various research works have reported partial solutions, none of these works so far has solved all the problems. Few studies aimed at the three problems of Li-metal at the same time, but recently, the research team of Professors Xia and Wang[220] addressed the above triplet of

Batteries & Supercaps

Review
doi.org/10.1002/batt.202200231

Chemistry Europe
European Chemical
Societies Publishing

problems. They used LLZTO solid-state electrolyte as an artificial SEI film to protect the Li-metal anode. The chemical and electrochemical properties of LLZTO solid-state electrolytes are very stable, and this kind of solid-state electrolyte is an excellent lithium-ion conductor. Therefore, they dispersed LLZTO powder in isopropanol by ultra-sonification, then dropped it on copper foil, and finally dried it under vacuum at 80°C to obtain a Cu foil-LLZTO electrode. The Cu foil-LLZTO electrode sheet is sintered at 900°C for 4 hours under the protection of argon atmosphere to obtain Cu foil-LLZTO-900. They believe that the Cu foam-LLZTO-900 electrode has excellent performance for lithium deposition and can be well applied in full batteries. The cycle performance comparison of Li symmetrical cells with different artificial SEI is shown in Table 1.

Generally speaking, artificial SEI can significantly increase the electrochemical efficiency performance for Li-metal batteries, but when the lithium content of the battery is high, the ionic conductivity and structural stability of the artificial SEI are often not satisfactory. There is a need to further study artificial SEI to promote the development of Li-metal anode protection strategies.

4.5. Other strategies for protecting Li-metal anodes

4.5.1. New methods to inhibit lithium dendrites: stress relief

Three-dimensional current collector, electrolyte additives, solid-state electrolyte, artificial SEI films and other methods to inhibit lithium dendrites have been introduced above. These methods often try to control any dendrites produced by applying chemical or physical methods but cannot prevent the formation of dendrites from the source mechanisms. Recently, Jiang et al.[221] discovered a new mechanism to inhibit lithium dendrites, which is a stress relief strategy. It is a widely observed phenomenon that the electrochemical deposition of metals produces compressive stress (especially noticeable in some electrodes such as Zn and Sn). However, whether metallic lithium also generates compressive stress during electrochemical deposition is still an unexplored question. Jiang et al.[221] studied the structure of copper/PDMS soft substrates and found that metallic lithium also generates stress on the surface of the current collector throughout the electrochemical deposition. This compressive stress is the main factor that causes the

enlargement of lithium dendrites. Therefore, if the compressive stress can be removed, the lithium dendrite growth will be effectively suppressed. The metal films on soft base materials will lose stability under compressive stress and form wrinkles to release the stress. In contrast, in a hard copper foil, the pressure stress caused by lithium plating cannot be relaxed, resulting in the development of lithium tree dendrites. Based on those, they successfully released compressive stress by allowing the soft substrate to lose its stability and achieved dendrite-free lithium deposition.[221]

Since the inhibition mechanisms against lithium dendrites found in this work come from the stress relief, approach this method may be complementary to other lithium dendrite inhibition mechanisms. Hence, there is a new feasible way to further improve the execution of Li-metal anodes in the future by enabling multiple mechanisms to simultaneously or sequentially suppress lithium dendrites.

4.5.2. Lithium anode inhibits with optimal structures

It can be seen from the above that the introduction of 3D frameworks as a host for metal lithium anodes has achieved excellent results. The majority of composite Li-metal anodes that have achieved good results were tested in symmetric structure designs. However, in practical applications, the two sides of the lithium metal foil contact with different battery components. The separator is on one side, while the current collector is on the other side. Therefore, the requirements and functions of the two sides are completely different. For an ideal anode structure, the side facing the separator should facilitate the transport of lithium-ion and have good compatibility to practice a balanced SEI film. Meanwhile, the other side of the Li-metal anodes facing the current collector should have good electrical contact and higher conductivity. The typical symmetric electrode generally does not consider the diverse constraints on both sides of the Li-metal anodes. Recently, Zhou et al.[222] reported a Mo net/Li metal film (MLF) composite electrode, which was established by an inverted thermal infusion method. The upper surface of this electrode has a dense oxide passivation layer, while the lower surface has a porous conductive structure formed by a Mo mesh matrix, and the active lithium layer is located between the upper and lower surfaces. The manufacturing process of this MLF composite electrode is shown in Figure 9(a). The total thickness of this

Table 1. The cycle performance comparison of Li symmetrical cells with different artificial SEI.

SEI strategy	Electrolyte	Cycle condition	Cycle life
LiF derived from Li/F_2[198]	1 M $LiPF_6$ in EC/DEC	1 mA cm^{-2}, 1 mAh cm^{-2}	200 cycles
LiF derived from Li/F_2[199]	1 M $LiPF_6$ in EC/DEC	1 mA cm^{-2}, 1 mAh cm^{-2}	600 h
LIF/Cu (MCI)[200]	1 M LiTFSI in DOL/DME	2.5 mA cm^{-2}, 0.5 mAh cm^{-2}	830 h
Li_2S/Li_2Se[207]	ether organic solvent (DOL:DME = 1:1) s	1.5 mA cm^{-2}, 3 mAh cm^{-2}	900 h
PTMEG-Li/Snpolymer-alloy mixed layer[215]	1 M LiTFSI in DOL/DME with 1 wt% $LiNO_3$	1 mA cm^{-2}, 1 mAh cm^{-2}	1000 h
Li_2S[219]	1 M $LiPF_6$ in EC/DEC	2 mA cm^{-2}, 5 mAh cm^{-2}	750 h
LLZTO-modified Cu foam[220]	1 M LiTFSI and 2 wt% LiNO3 in DOL/DME	0.5 mA cm^{-2}, 0.5 mAh cm^{-2}	2400 h

Batteries & Supercaps

Review
doi.org/10.1002/batt.202200231

Chemistry Europe
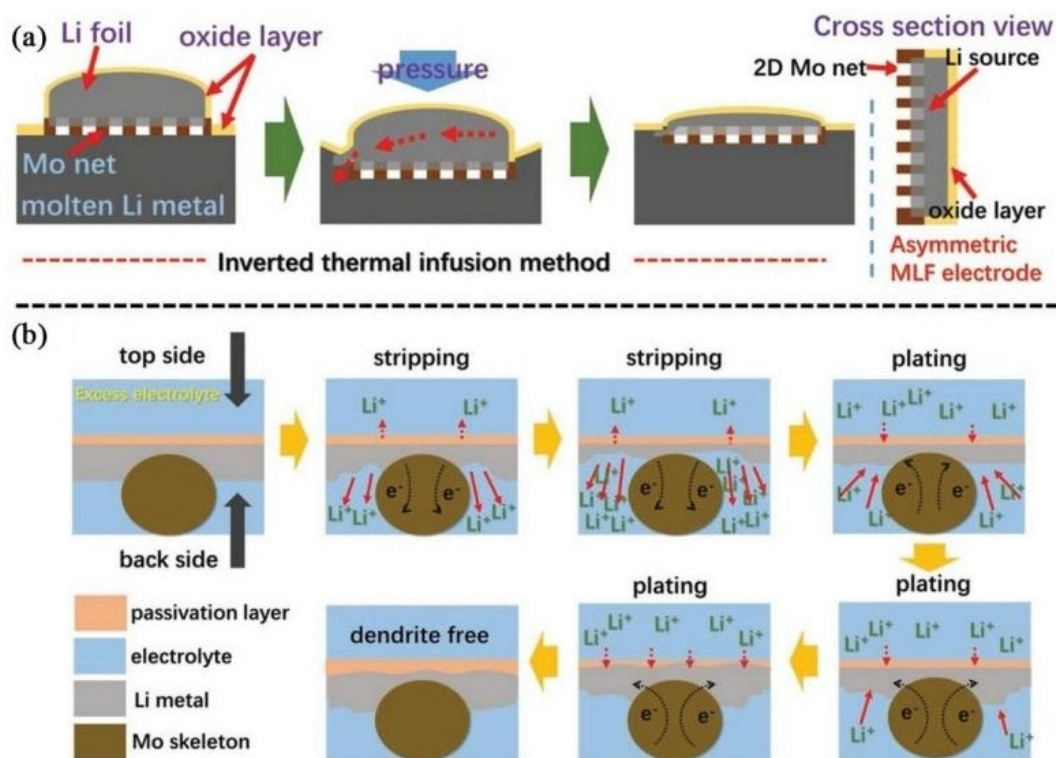European Chemical
Societies Publishing

Figure 9. a) Schematic of the fabrication process of MLF electrodes. b) Schematic diagram of the Li stripping/plating behavior on an MLF electrode. Reproduced with permission from Ref. [222]. Copyright (2019) Wiley-VCH.

asymmetric MLF electrode is only 90 μm, and the thickness of the lithium film is about 40 μm, which is lower than other composite metal lithium anodes reported. Throughout the lithium plating/stripping method, the lithium oxide layer on the upper surface of the MLF electrode functions as an artificial SEI layer, which maintains the stability of the SEI interface. As shown in Figure 9(b), after sufficient electrolyte penetrates the MLF electrode, lithium deposition/stripping behavior occurs preferentially on the back of the electrode at a relatively high current density, thereby forming a unique "top-down" lithium deposition. Furthermore, the porous nature of the molybdenum mesh gives sufficient space for the electrode's volume change. With this asymmetric scheme, the growth of lithium dendrites was effectively reduced. MLF electrodes show excellent electrochemical efficiency including both symmetrical batteries and lithium-sulfur full batteries. This research proposes a new design concept for high-performance composite metal lithium anodes.[222]

In addition to designing asymmetric Li-metal anodes, Li et al.[223] also constructed a novel upright Li-metal anode with improved safety and stability. They cut glass fiber membrane and lithium foil into thin strips about 1.5 mm wide, stacked them up and down, and wound them from left to right to prepare a Li-metal anode with a vertical structure. According to calculations, the surface area of this upright structure has increased 4 times compared with the planar structure and has fewer outer surfaces and more inner surfaces exposed, which is beneficial to facilitate internal lithium deposition. Combining

the high lithium affinity and liquid absorption of the glass fiber membrane, this Li-metal anode has several advantages. Firstly, the preparation process is simple and easy to replicate. In addition, the abundant internal reaction interface and the good lithium affinity of the glass fiber at the interface can encourage the deposition of Li-metal inside the electrode structure. Furthermore, the glass fiber interlayer with higher porosity allows for increased lithium storage space, reducing the anode's volume expansion and avoid short-circuiting of batteries. Moreover, the high liquid absorption rate of glass fiber can maintain a durable Li supply and transmission inside the electrode, preventing the battery from drying out and extending the cycle life of the anodes.[222] The Li-metal anodes with this unique structure can still maintain excellent cycle stability under high current density. Li et al.'s research has brought new research directions for the optimization of lithium anodes. If the outer surface of the anodes can be further passivated and the inner surface reaction activity can be simultaneously improved, it is expected to completely change the lithium deposition direction and significantly enhance the stability and safety of Li-metal anodes.

Batteries & Supercaps

Review
doi.org/10.1002/batt.202200231

Chemistry
Europe
European Chemical
Societies Publishing

5. Study on Environmental Stability of Lithium-Metal Anodes

The practical applications of lithium anodes in high-energy batteries require the improvement of stability in various environment. The following section summarizes the strategies that have been developed recently to increase the stability of Li metal anodes when expose to atmosphere.

5.1. Strategies to improve the stability of lithium metal anodes in the atmosphere

It is well known that the high reactivity of lithium metal limits the practical application of lithium anodes. Lithium is easily corroded in the air, generating uneven passivation layers such as LiOH, Li_2CO_3, and Li_3N on the surface, which can seriously degrade its performance.[223] In addition, when lithium encounters humid air and water, it can cause safety issues due to the generation of large amounts of hydrogen and heat.[224] Therefore, to avoid these situations, extremely dry air environments or high-purity inert gases are required, which represent a huge increase in cost during the battery fabrication process, thus greatly limiting the development of high-density lithium-metal batteries. Construct of protective layers or surface treatment on the Li-metal anodes is one of the most effective and widely applied methods.

Qu et al.[225] used magnetron sputtering to deposit Al thin film on the surface of Li foil as a protective layer. The formation of dense aluminum film effectively prevents the lithium metal anode from contact with moisture and oxygen in the air, and the coating layer has a good passivation effect on the lithium metal anode, resulting in reduced impedance. Therefore, this Al-coated lithium metal electrode exhibited high stability in air and carbonate-based electrolytes. The symmetrical cells with aluminum-coated lithium metal electrodes can be cycled for 950 h at $0.5\ mA\ cm^{-2}$ and $0.5\ mAh\ cm^{-2}$. Ma et al.[226] used inert high-quality chemical vapor deposition (CVD) graphene layer to passivate the lithium surface, which was able to solve the problems of air stability and electrochemical stability of lithium metal anode at the same time. Due to the high crystallinity and hydrophobicity of the CVD graphene layer, the prepared waterproof graphene-coated Li (gLi) even presented reactions with water. This graphene coating with excellent conductivity and mechanical properties can effectively dissipate local surface charge, homogenize lithium deposition, inhibit dendrite growth, and protect lithium surface from parasitic reactions with organic electrolytes and water, thus solving the problems of air stability and electrochemical stability. Li-air batteries fabricated with the gLi anode can be cycled for 2300 hours with the capacity limitation of $1000\ mAh\ g^{-1}$ at the current density of $200\ mA\ g^{-1}$. More importantly, the recycled anode can be recombined with a new cathode and run for another 400 hours.

Wang et al.[227] prepared a robust moist-air-stable polymer-LiF-alloy hybrid hierarchical layer (MASPLA-Li) by a chemical method from the perspective of multifunctional design of the surface interface. The protective layer is prepared by carefully tuning the precursor concentration and self-reaction time. The formed protective layer is a homogeneous, non-porous and thin film. Therefore, it can resist corrosion by moisture without sacrificing lithium ion diffusion capability and energy density. At the same time, the Li anode treated with MASPLA modulation layer acquires higher hydrophobicity and maintains a smooth surface. The alloy layer promotes rapid ion/atom diffusion, achieves uniform nucleation of the lithium metal, and forms a uniform lithium plating layer, resulting in an extended plating life of the MASPLA-Li anode to more than 600 h with an overpotential of $\sim 10\ mV$ and a high Coulombic efficiency of about 99.3% in moist air. The capacity of the Li-S cell with MASPLA-Li anode is $656\ mAh\ g^{-1}$, and the cycling stability and rate performance were also effectively improved compared with the cell with the pristine lithium anode. This method enhances the practical and scalable production of Li metal cathodes in humid air, and the prepared cells can be stably cycled hundreds of times and realize the initial application of high surface density batteries. Recently, Wang et al.[227] used methacryloxypropyltrimethoxysilane, an inexpensive silane coupling agent, to modify lithium metal to achieve reinforced SEI film, which made lithium metal resistance to air oxidation in one stroke. This dense modified layer can effectively resist air erosion, enhance the stability of lithium metal in air, reduce the high requirement of air humidity in the production process of lithium metal batteries, and lower the cost of commercialization. In addition, the silicon functional group of MPS can form a strong Li–O–Si chemical bond on the surface of lithium metal, and the organic functional group of MPS has a physical entanglement effect with the SEI film, thus achieving SEI film reinforcement. The MPS-Li||MPSLi symmetric cell can be cycled stably at a current density of $1\ mA\ cm^{-2}$ for 1400 h. This method adopts the principle that silane coupling agents can bond materials with different properties and applies it to the field of lithium metal electrodes. It also shows the direction to investigate the different effects of silane coupling agents with different functional groups and SEI films.

Although Li-metal cells protected by artificial films have made great progress in terms of air stability, these processes often require dedicated equipment and high prices and are not suitable for commercial development. Therefore, there is a need to develop simpler, less expensive methods that can be produced on a large scale.

5.2. The influence of temperature on the lithium anodes

More and more electronic devices and electric vehicles are being used in harsh environments. As a crucial component of the next generation of high specific energy Li-metal batteries, it is critical to investigate the thermal properties of Li-metal. Li metal anodes have a substantial impact on the performance of both Li-sulfur and Li-air batteries. Wang et al.[231] investigated the nucleation and deposition behavior of Li-metal anodes at temperatures ranging from -20 to $60\,°C$. This work reveals

high-temperature conditions inducing the formation of uneven (i.e., randomly sparse and dense) lithium deposits. As shown in Figure 10a, by elevating the temperature from −20 °C to 60 °C, at the same current density, the size of lithium nuclei increases, and their density also decreases. Figure 10b shows the *in situ* lithium nucleation and growth processes at 60 °C and 20 °C at the same current density (0.5 mA cm⁻²). The in situ optical observations demonstrate that the details of Li nucleation are significantly affected through the operating temperature. Further cryo-electron microscopy characterization is shown in Figure 10(c and d), indicating the thickness of the SEI layer decreases from 23 nm at 60 °C to 17 nm at 20 °C. Therefore, increasing the temperature can significantly change the structure and composition of solid-state electrolyte SEI layers. High-temperature working conditions can considerably increase the electrochemical efficiency including both half-cell and full-cell batteries. To investigate the electrochemical performance of lithium anodes at different temperatures, Li‖Cu half cells were tested at 0.5 mA cm⁻² with an areal capacity of 1 mAh cm⁻². An operating temperature change from 20 °C to 60 °C can achieve a four-fold increase in cyclability and the average Coulombic efficiency is increased from 97.7 % at 20 °C to 98.9 % at 60 °C (Figure 10e). When Li electroplating/stripping is performed at high temperature, the over-potential decreases as well (Figure 10f). To further study the effect of temperature on the electrochemical behavior of Li-metal anodes, Li‖Li symmetric cells have been further investigated. Figure 10(g) indicates that symmetric cells operating at 60 °C have a lifespan that is more than double that of cells operating at 20 °C. The

creation of SEI and the accumulation of "dead" lithium during cycling are the main causes of low Coulombic efficiency and poor cycling performance in lithium anodes.[232] The overhead experimental outcomes show that higher temperature is conducive to reversible lithium electroplating/stripping and reduces the side reactions from SEI formation and efficiently inhibits the generation of "dead" Li. In Figure 10(h), it can be observed that the cycle life of the cell operated at 60 °C is significantly longer than that at 20 °C, and the energy efficiency is significantly improved. Hence, Wang et al.[231] have demonstrated the practicability of elevated temperature promoting, rather than degrading, the performances of Li-metal-based full cells. In conclusion, combined with systematic observation, in-situ characterization, and theoretical simulations, this work elucidated the mechanism of temperature-induced changes in Li-metal deposition behavior. High temperature promotes the diffusion and transfer of lithium ions in the electrolyte and the solid-state electrolyte membrane. Faster-moving lithium ions can decrease the number of nucleation points and increase the volume of lithium nuclei. At high lithium deposition capacity, the lithium particles at high temperatures gradually fuse to form a dense and flat lithium deposition layer. Under low-temperature conditions, the slower diffusion rate of lithium-ions point out to an enhanced in nucleation points and a reduction in the size of lithium nuclei. Meanwhile, the continuous deposition will form a loose lithium deposition layer and possibly lithium dendrites. Compared with a single amorphous SEI formed at room temperature, the SEI formed at high temperature has an additional Li_2O outer layer, which
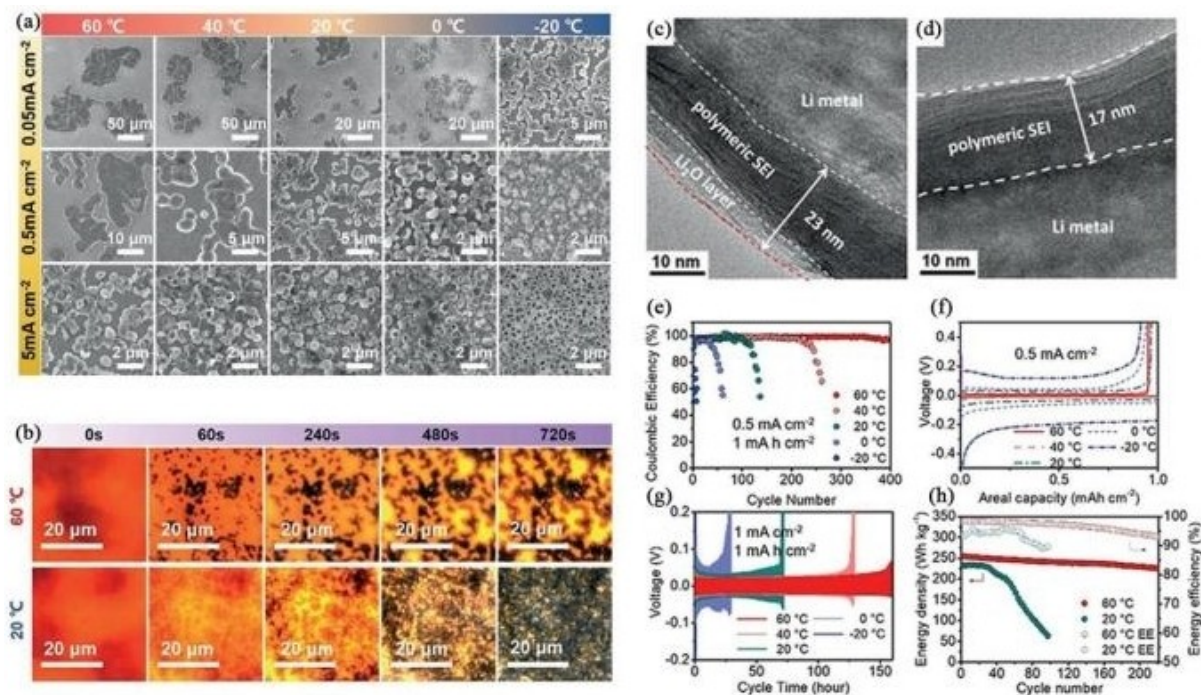

Figure 10. a) SEM images of Li nucleation layers under different temperature conditions. b) In situ optical images of Li nuclei growth at 20 °C and 60 °C. c) Cryo-EM images of SEI formed at 60 °C and d) 20 °C. e) Coulombic efficiencies of Li plating/stripping on Cu at different temperatures. f) The first cycle voltage profiles of Li plating/stripping. g) Charge/discharge voltage profiles of Li‖Li symmetric cells. h) Energy density and energy efficiency of Li‖LTO full cells at 60 °C and 20 °C. Reproduced with permission from Ref. [231]. Copyright (2019) Wiley-VCH.

Batteries & Supercaps

Review
doi.org/10.1002/batt.202200231

Chemistry Europe
European Chemical
Societies Publishing

significantly increases the stability of the SEI. This work carefully revealed the influence of temperature on Li-metal anode and, more importantly, proved the effectiveness and feasibility of high temperatures to improve battery performance. At the same time, this work has laid a solid theoretical and experimental foundation for the sake of ongoing growth and application of Li-metal batteries.

Wang et al.[231] explored the performance of Li-metal in ether-based electrolytes at different temperatures. Although ether-based electrolytes are very suitable for low operating voltage battery systems (e.g., Li-S batteries), however, the lower oxidation voltage limits their application in work systems with high operating voltages. Carbonate-based electrolytes have a wider electrochemical stability window than ether-based electrolytes, so Carbonate-based electrolytes can be relatively better matched to the cathode material of the cell in such operating systems, so they are also considered very important in battery systems. Li-metal is thermodynamically unstable with carbonate-based electrolytes, so the behavior of the Li-metal electrode interface in carbonate-based electrolytes can be

significantly different from that of ether-based electrolytes.[232] An in-depth understanding of the electrochemical properties of Li-metal in carbonate-based electrolytes at different temperatures and the mechanism is a blind spot in current research. Although there have been many reports on different characterization methods for Li-metal anodes, including electron microscopy, electrochemical impedance spectroscopy, and photoelectron spectroscopy, it is often difficult to get a clear and complete understanding of the specific relationship between interface chemistry and topography. Based on these, Sun et al.[233] have adopted a series of synchrotron radiation characterization techniques, including synchrotron radiation X-ray fluorescence mappings (XRF mappings), X-ray absorption near edge structure (XANES) and X-ray computed tomography, combined with other chemical and electrochemical characterization methods. They achieved a depth of insight into the cycling working and reaction mechanisms of Li-metal anodes at different temperatures. The SEM images of the different stages of Li metal development on a Li metal surface are shown in Figure 11(a). They successfully identified four main growth
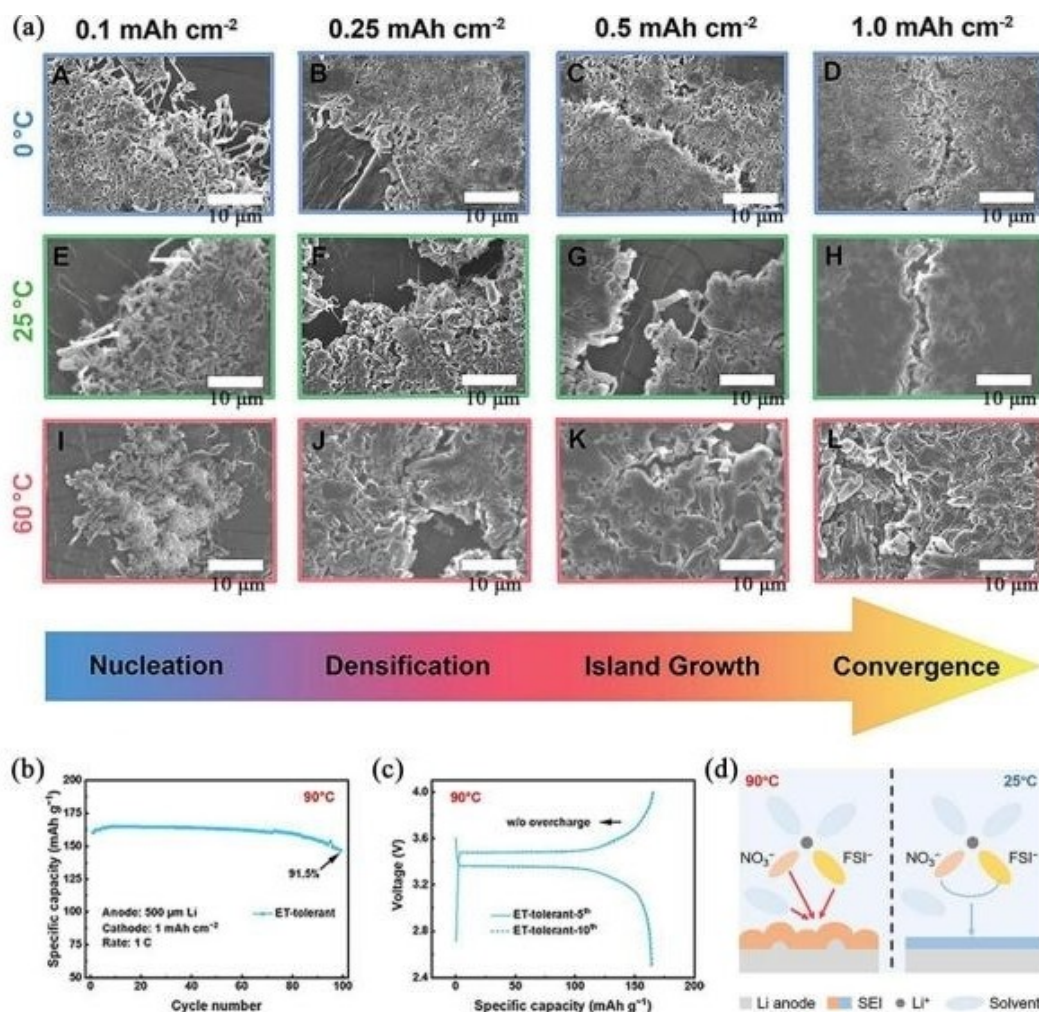

Figure 11. a) SEM images of the different stages of Li metal growth on a Li metal surface. Scale bars in all images are 10 μm. Reproduced with permission from Ref. [233]. Copyright (2020) Wiley-VCH. b and c) Electrochemical performance of Li│LiFePO₄ batteries with an ET-tolerant electrolyte at 90 °C. d) The SEI formation mechanisms at 90 and 25 °C. Reproduced with permission from Ref. [234]. Copyright (2020) Wiley-VCH.

Batteries & Supercaps

Review
doi.org/10.1002/batt.202200231

Chemistry Europe
European Chemical
Societies Publishing

stages relevant to all temperature test conditions: nucleation, densification, island growth, and convergence. Temperature obviously has an impact not only on the early nucleation morphology but also on the long-term plating/stripping behavior. In this work, it was found that Li-metal has higher Coulombic efficiency and cycle life in carbonate-based electrolytes at low temperatures. In contrast, at high temperatures, the stability of Li-metal anodes decreased due to more critical side reactions with the electrolyte. This work make available first-hand ideas for characterization approaches and practical applications of Li-metal anodes. However, a deeper understanding of the electrochemical performance and mechanism of Li-metal in carbonate-based electrolytes at different temperatures is still a blind spot in current research.[233]

It is well-known that the carbonate-based electrolyte decomposes above 55 °C, and the SEI on the anode surface decomposes above 65 °C, resulting in rapid battery capacity decay and battery failure. The requirement for nonaqueous liquid electrolytes is also increasing owing to the higher reactivity of lithium. And the need for lithium batteries to be used in extreme environments is also increasing. Zhang et al.[234] also studied the feasibility of Li metal anodes working at 90 °C and the changes of SEI on the surface of Li-metal anodes at such an elevated working temperature. They use a higher temperature-tolerant (ET-tolerant) electrolyte, which enabled Li | LiFePO$_4$ batteries to be recharged 100 times at 90 °C (which is shown in Figure 11b), while batteries that use conventional carbonate electrolytes can only be cycled ten times. And it can easily Figure out from Figure 11(c) that there is nearly no overcharge during repeated cycles. The high temperature will cause the self-governing and imperfect decomposition of the lithium salt and the solvent, thereby expressively changing the composition of the SEI. At high temperatures, unstable intermediate decomposition products appear in the SEI, and the content of LiF and other components that contribute to lithium-ion transmission significantly decreases. Therefore, the formed SEI has a high ion transport resistance, and this resistance is unevenly distributed throughout the material, resulting in uneven deposition of Li-metal (Figure 11d).[234] This work not only proves the possibility of Li-metal anode cycling at 90 °C but also offers new insights into the SEI and lithium deposition behavior of metallic lithium surfaces at high temperatures.

In conclusion, high temperature shows significant improvement effect on the performance of lithium anodes in ether-based electrolytes, while the stability and electrochemical performance of lithium anodes in carbonate electrolytes are still not satisfied at high temperature. The insight into the mechanical study of lithium metal anodes at different temperatures requires further investigation, and improvement strategies are needed to further promote the development of high-energy-density lithium metal batteries.

6. Summary and Perspective

Lithium-metal batteries are thought to be an encouraging next-generation high-energy-density energy storage device, but for large-scale practical applications, the entire battery system still requires further development. In particular, any constant growth of lithium dendrites during cycling can penetrate a separator membrane, ensuing in a short circuit of the battery. To solve this problem, in the past 40 years, researchers have proposed a variety of models to recognize the nucleation and dendrite growth mechanism during lithium deposition processes. Two major factors which control the evolution of lithium dendrites have been identified. One is the low surface energy of lithium, which makes lithium tend to grow into one-dimensional dendrites. The other is that the diffusion rate of lithium ions in an uneven SEI layer is slow, which promotes continuous lithium dendrite growth at the position of any surface protrusions. A Li-metal anode is more likely to generate dendrites under the conditions of high current and low temperature. In addition, any unlimited volume expansion of Li-metal anodes will lead to the generation of dead lithium, thereby reducing the utilization rate of the active materials. Our work encapsulates the improvement approaches for Li-metal anodes in recent years, including optimizing electrolyte components, using solid-state electrolytes, introducing artificial SEI, designing 3D lithium storage frameworks and current collector. As well as ensuring the practical application of Li-metal batteries by creating a protective layer to improve the air stability of the lithium anode and regulating the operating temperature.

Although many exciting results have been achieved in the research on Li-metal anode protection strategies, some problems still need to be resolved for future practical application.

At present, the theoretical studies of Li-metal anodes are still in an initial stage, and there is much room for exploration in both theoretical and practically-related research. The currently proposed models are limited to a few specific conditions. For example, the space charge model and heterogeneous nucleation model, have not considered the electrolyte decomposition and SEI formation during the deposition process. These factors will affect the steps of lithium nucleation and deposition. In addition, each model is suitable for only a narrow range of specific steps of lithium deposition, which has been proved by specially designed experiments. A more general mechanism should be established to describe the entire process of lithium dendrite growth. An in-depth understanding of lithium plating behavior will help minimize or eliminate lithium dendrites.

In work on Li-metal anodes, researchers have made many breakthroughs, but they are mainly at the laboratory scale and are still far from large-scale industrial production. Also, research on various aspects of high-energy Li-metal batteries remains challenging, and many issues need to be understood in deeper detail.

At present, the formation mechanisms, structure, composition, and regulation of SEI still need to be further studied, and the growth of lithium dendrite largely based on the application

Batteries & Supercaps

Review
doi.org/10.1002/batt.202200231

Chemistry Europe
European Chemical
Societies Publishing

mode and current density of the battery. These conditions are variable in practical applications. Furthermore, enhancing the Coulombic stability and efficiency of Li-metal anodes is also an urgent problem. Now is quite a "golden age" for rechargeable batteries aimed at renewable energy storage and electric transportation. This era with rapid scientific progress has provided many technologies for the study and understanding of Li-metal anodes, including various in-situ and ex-situ techniques: AFM, HRTEM, NMR, cryo-electron microscopy, and other technologies. However, the rapid development of various technologies also means that the alternative systems to Li-metal anodes are also under simultaneous rapid development, which makes possible energy storage scenarios constantly changing. Rechargeable Li-metal batteries have very broad prospects, but we still need to undertake more studies on Li-metal anodes, both in terms of science and engineering.

Acknowledgements

Conflict of Interest

The authors declare no conflict of interest.

Data Availability Statement

The data that support the findings of this study are available from the corresponding author upon reasonable request.

[1] G. N. Lewis, F. G. Keyes, *J. Am. Chem. Soc.* **1913**, *35*, 340–344.
[2] L. L. Li, S. Y. Li, Y. Y. Lu, *Chem. Commun.* **2018**, *54*, 6648–6661.
[3] M. S. Whittingham, *Chem. Rev.* **2004**, *104*, 4271–4302.
[4] D. W. Murphy, F. J. D. Salvo, J. N. Carides, J. V. Waszczak, *Mater. Res. Bull.* **1978**, *13*, 1395–1402.
[5] M. Lazzari, B. Scrosati, *Chem. Informationsdienst* **1980**, *127*, 774.
[6] Z. Gao, H. Sun, L. Fu, F. Ye, F. Zhang, W. Luo, Y. Huang, *Adv. Mater.* **2018**, *30*, 1870122.
[7] J. M. Tarascon, M. Armand, *Nature* **2001**, *414*, 359–367.
[8] X. B. Cheng, C. Z. Zhao, Y. X. Yao, H. Liu, Q. Zhang, *Chem* **2019**, *5*, 74.
[9] B. Dunn, H. Kamath, J. M. Tarascon, *Science* **2011**, *334*, 928–935.
[10] S. Chu, A. Majumdar, *Nature* **2012**, *488*, 294–303.
[11] M. Armand, J. M. Tarascon, *Nature* **2008**, *451*, 652–657.
[12] Y. Liang, C. Z. Zhao, H. Yuan, Y. Chen, W. C. Zhang, J. Q. Huang, D. S. Yu, Y. L. Liu, M. M. Titirici, Y. L. Chueh, H. J. Yu, Q. Zhang, *InfoMat.* **2019**, *1*, 6–32.
[13] J. Janek, W. G. Zeier, *Nat. Energy* **2016**, *1*, 1667–1176.
[14] D. J. Aurbach, *J. Power Sources.* **2000**, *89*, 206–218.
[15] T. Y. Wang, Y. B. Li, J. Q. Zhang, K. Yan, P. Jaumaux, J. Yang, C. Y. Wang, D. Shanmukaraj, B. Sun, M. Armand, Y. Cui, G. X. Wang, *Nat. Commun.* **2020**, *11*, 1–9.
[16] P. G. Bruce, S. A. Freunberger, L. J. Hardwick, J. M. Tarascon, *Nat. Mater.* **2012**, *11*, 19–29.
[17] A. J. Louli, M. Coon, M. Genovese, M. J. DeGooyer, A. Eldesoky, J. R. Dahn, *J. Electrochem. Soc.* **2021**, *168*, 020515.
[18] R. L. Sacci, J. M. Black, N. Balke, N. J. Dudney, K. L. More, R. R. Unocic, *Nano Lett.* **2015**, *15*, 2011–2018.
[19] X. B. Cheng, R. Zhang, C. Z. Zhao, Q. Zhang, *Chem. Rev.* **2017**, *117*, 10403–10473.
[20] D. Wang, W. Zhang, W. T. Zheng, X. Q. Cui, T. Rojo, Q. Zhang, *Adv. Sci.* **2017**, *4*, 1600168–1600178.
[21] P. Y. Zhai, H. J. Peng, X. B. Cheng, L. Zhu, J. Q. Huang, W. Zhu, Q. Zhang, *Energy Storage Mater.* **2017**, *7*, 56–63.
[22] H. J. Peng, D. W. Wang, J. Q. Huang, X. B. Cheng, Z. Yuan, F. Wei, Q. Zhang, *Adv. Sci.* **2016**, *3*, 1500268.
[23] D. C. Lin, Y. Y. Liu, Y. Cui, *Nat. Nanotechnol.* **2017**, *12*, 194–206.
[24] J. M. Tarascon, M. Armand, *Nature* **2001**, *414*, 359–367.
[25] W. Xu, J. L. Wang, F. Ding, X. L. Chen, E. Nasybutin, Y. H. Zhang, J. G. Zhang, *Energy Environ. Sci.* **2014**, *7*, 513–437.
[26] Y. P. Guo, H. Q. Li, T. Y. Zhai, *Adv. Mater.* **2017**, *29*, 1700007–1700031.
[27] N. W. Li, Y. Shi, Y. X. Yin, X. X. Zeng, J. Y. Li, C. J. Li, L. J. Wan, R. Wen, Y. G. Guo, *Angew. Chem. Int. Ed.* **2018**, *57*, 1505–1509; *Angew. Chem.* **2018**, *130*, 1521–1525.
[28] J. Lee, D. A. Kitchaev, D. H. Kwon, C. W. Lee, J. K. Papp, Y. S. Liu, Z. Lun, R. J. Clement, T. Shi, B. D. McCloskey, J. Guo, M. Balasubramanian, G. Ceder, *Nature.* **2018**, *556*, 185–190.
[29] L. Ma, M. S. Kim, L. A. Archer, *Chem. Mater.* **2017**, *29*, 4181–4189.
[30] J. D. Huang, J. D. Liu, J. He, M. G. Wu, S. H. Qi, H. P. Wang, F. Li, J. M. Ma, *Angew. Chem.* **2021**, *13*, 20717–20722.
[31] X. Li, J. Liu, J. He, S. Qi, M. Wu, H. Wang, J. Ma, *Adv. Sci.* **2022**, *15*, 2201297.
[32] B. R. Wygant, L. C. Merrill, K. L. Harrison, A. A. Talin, D. S. Ashby, T. N. Lambert, *Adv. Sci.* **2022**, *9*, 2105803.
[33] L. Zhang, M. Al-Mamun, *Green Energy & Environ.* **2022**, *7*, 173–175.
[34] S. Zhang, B. Cheng, Y. Fang, D. Dang, X. Shen, Z. Li, Q. Liu, *Chin. Chem. Lett.* **2022**, *33*, 3951–3954.
[35] Y. N. Li, C. Y. Wang, R. M. Gao, F. F. Cao, H. Ye, *Energy Storage Mater.* **2021**, *38*, 262–275.
[36] Q. Sun, X. Chen, J. Xie, C. Huang, X. Xu, J. Tu, C. Shen, Y. Jin, K. Zhang, F. Chene, T. Zhu, X. Zhao, J. Cheng, *Mater. Today Nano* **2022**, *19*, 100235.
[37] M. Liu, S. Ganapathy, M. Wagemaker, *Acc. Chem. Res.* **2022**, *55*, 333–344.
[38] M. J. Lee, J. Han, K. Lee, Y. J. Lee, B. G. Kim, K. N. Jung, S. W. Lee, *Nature* **2022**, *601*, 217–222.
[39] Z. Li, S. Wang, J. Shi, Y. Liu, S. Zheng, H. Zou, Q. Zheng, *Energy Storage Mater.* **2022**, *47*, 262–270.
[40] F. Ding, W. Xu, G. L. Graff, J. Zhang, M. L. Sushko, X. L. Chen, Y. Y. Shao, M. H. Engelhard, Z. M. Nie, J. Xiao, X. J. Liu, P. V. Sushko, J. Liu, J. G. Zhang, *J. Am. Chem. Soc.* **2013**, *135*, 4450–4456.
[41] J. N. Chazalviel, *Phys. Rev. A* **1990**, *42*, 7355–7367.
[42] C. Brissot, M. Rosso, J. N. Chazalviel, S. J. Lascaud, *J. Power Sources* **1999**, *81*, 925–929.
[43] V. Fleury, J. N. Chazalviel, M. Rosso, B. Sapoval, *Electroanal. Chem. Interfacial Electrochem.* **1990**, *290*, 249–255.
[44] M. Rosso, C. Brissot, A. Teyssot, M. Dolle, L. Sannier, J. M. Tarascon, R. Bouchetc, S. Lascaud, *Electrochim. Acta.* **2006**, *51*, 5334–5340.
[45] S. Lv, T. Verhallen, A. Vasileiadis, F. Ooms, Y. Xu, Z. Li, Z. Li, M. Wagemaker, *Nat Commun.* **2018**, *9*, 2152–2163.
[46] J. Yamaki, S. Tobishima, K. Hayashi, K. Saito, Y. Nemoto, M. J. Arakawa, *J. Power Sources* **1998**, *74*, 219–227.
[47] D. R. Ely, R. E. Garcia, *J. Electrochem. Soc.* **2013**, *160*, A662-A668.
[48] A. Pei, G. Zheng, F. Shi, Y. Li, Y. Cui, *Nano Lett.* **2017**, *17*, 1132–1139.
[49] J. Liu, Z. Bao, Y. Cui, E. J. Dufek, J. B. Goodenough, P. Khalifah, Q. Li, B. Y. Liaw, P. Liu, A. Manthiram, et al., *Nat. Energy.* **2019**, *4*, 180–186.
[50] X. Sun, X. Zhang, Q. Ma, X. Guan, W. Wang, W. Luo, *Angew. Chem. Int. Ed.* **2020**, *59*, 6665–6674; *Angew. Chem.* **2020**, *132*, 6730–6739.
[51] J. H. Jeong, N. Goldenfeld, J. A. Dantzig, *Phys. E* **2001**, *64*, 041602.
[52] C. Ling, D. Banerjee, M. Matsui, *Electrochim. Acta* **2012**, *76*, 270–274.
[53] M. Jaeckle, A. J. Gross, *Chem. Phys.* **2014**, *141*, 174710–174717.
[54] K. J. Harry, D. T. Hallinan, D. Y. Parkinson, A. A. MacDowell, N. P. Balsara, *Nat. Mater.* **2014**, *13*, 69–73.

Batteries & Supercaps

Review

doi.org/10.1002/batt.202200231

Chemistry
Europe

European Chemical
Societies Publishing

[55] T. M. Arruda, J. S. Lawton, A. Kumar, R. R. Unocic, I. I. Kravchenko, T. A. Zawodzinski, S. Jesse, S. V. Kalinin, N. Balke, *ECS Electrochem. Lett.* **2013**, *3*, A4-A9.

[56] E. Kazyak, K. N. Wood, N. P. Dasgupta, *Chem. Mater.* **2015**, *27*, 6457–6462.

[57] J. Liu, Y. Wang, F. Liu, F. Cheng, J. Chen, *J. Energy Chem.* **2020**, *42*, 1–4.

[58] D. Lu, Y. Shao, T. Lozano, W. D. Bennett, G. L. Graff, B. Polzin, J. Zhang, M. H. Engelhard, N. T. Saenz, W. A. Henderson, P. Bhattacharya, J. Liu, J. Xiao, *Adv. Energy Mater.* **2015**, *5*, 1400993–1400996.

[59] P. Biawal, S. Stalin, A. Kludz, S. Choudhury, L. A. Archer, *Nano Lett.* **2019**, *19*, 8191–8200.

[60] A. S. Westover, N. J. Dudney, R. L. Sacci, S. Kalnaus, *ACS Energy Lett.* **2019**, *4*, 651–655.

[61] Q. Li, T. Yi, X. Wang, H. Pan, B. Quan, T. Liang, X. Guo, X. Yu, H. Wang, X. Huang, L. Chen, H. Li, *Nano Energy* **2019**, *63*, 103895.

[62] Y. Li, Y. Li, A. Pei, K. Yan, Y. Sun, C. L. Wu, L. M. Joubert, R. Chin, A. L. Koh, Y. Yu, J. Perrino, B. Butz, S. Chu, Y. Cui, *Science* **2017**, *358*, 506–510.

[63] Z. Ju, J. Nai, Y. Wang, T. Liu, J. Zheng, H. Yuan, O. Sheng, C. Jin, W. Zhang, Z. Jin, H. Tian, Y. Liu, X. Tao, *Nat. Commun.* **2020**, *11*, 488–452.

[64] A. J. Leenheer, K. L. Jungjohann, K. R. Zavadil, J. P. Sullivan, C. T. Harris, *ACS Nano* **2015**, *9*, 4379–4389.

[65] Z. Zeng, W. I. Liang, H. G. Liao, H. L. Xin, Y. H. Chu, H. Zheng, *Nano Lett.* **2014**, *14*, 1745–1750.

[66] B. L. Mehdi, J. Qian, E. Nasybulin, C. Park, D. A. Welch, R. Faller, H. Mehta, W. A. Henderson, W. Xu, C. M. Wang, J. E. Evans, J. Liu, J. G. Zhang, K. T. Mueller, N. D. Browning, *Nano Lett.* **2015**, *15*, 2168–2173.

[67] O. Sheng, J. Zheng, Z. Ju, C. Jin, Y. Wang, M. Chen, J. Nai, T. Liu, W. Zhang, Y. Liu, X. Tao, *Adv. Mater.* **2020**, *32*, 2000223–2000229.

[68] Y. S. Cohen, Y. Cohen, D. Aurbach, *J. Phys. Chem. B* **2000**, *104*, 12282–12291.

[69] L. Zhang, T. Yang, C. Du, Q. Liu, Y. Tang, J. Zhao, B. Wang, T. Chen, Y. Sun, P. Jia, H. Li, L. Geng, J. Chen, H. Ye, Z. Wang, Y. Li, H. Sun, X. Li, Q. Dai, Y. Tang, Q. Peng, T. Shen, S. Zhang, T. Zhu, J. Huang, *Nat. Nanotechnol.* **2020**, *15*, 94–98.

[70] C. Yu, S. Ganapathy, E. R. H. v. E. Wang, S. Basak, Z. Li, M. Wagemaker, *Nat. Commun.* **2017**, *8*, 1086–1089.

[71] C. Fiedler, B. Luerssen, M. Rohnke, J. Sann, J. Janek, *J. Electrochem. Soc.* **2017**, *164*, A37-A42.

[72] X. B. Cheng, R. Zhang, C. Z. Zhao, Q. Zhang, *Chem. Rev.* **2017**, *117*, 10403–10473.

[73] R. Zhang, X. B. Cheng, C. Z. Zhao, H. J. Peng, J. L. Shi, J. Q. Huang, J. Wang, F. Wei, Q. Zhang, *Adv. Mater.* **2016**, *28*, 2155–2162.

[74] X. B. Cheng, H. J. Peng, J. Q. Huang, F. Wei, Q. Zhang, *Small.* **2014**, *10*, 4257–4263.

[75] N. Nitta, F. X. Wu, J. T. Lee, G. Yushin, *Mater. Today* **2015**, *18*, 252–264.

[76] Z. S. Wu, W. C. Ren, L. Xu, F. Li, H. M. Cheng, *ACS Nano.* **2011**, *5*, 5463–5471.

[77] X. Nie, A. Zhang, Y. Liu, C. Shen, M. Chen, C. Xu, Q. Liu, J. Cai, A. Alfaraidi, C. Zhou, *Energy Storage Mater.* **2019**, *17*, 341–348.

[78] H. Yadegari, M. A. Koronfel, K. Wang, D. B. Thornton, I. E. L. Stephens, C. Molteni, P. D. Haynes, M. P. Ryan, *ACS Energy Lett.* **2021**, *6*, 1633–1638.

[79] J. Zhao, G. Zhou, K. Yan, J. Xie, Y. Li, L. Liao, Y. Jin, K. Liu, P. C. Hsu, J. Wang, H. M. Cheng, Y. Cui, *Nat. Nanotechnol.* **2017**, *12*, 993–999.

[80] P. Xue, S. Liu, X. Shi, C. Sun, C. Lai, Y. Zhou, D. Sui, Y. Chen, J. Liang, *Adv. Mater.* **2018**, *30*, 1804161–1804172.

[81] B. Z. Yu, T. Tao, S. Mateti, S. G. Lu, Y. Chen, *Adv. Funct. Mater.* **2018**, *28*, 1803023–1803031.

[82] R. Zhang, X. R. Chen, X. Chen, X. B. Cheng, X. Q. Zhang, C. Yan, Q. Zhang, *Angew. Chem.* **2017**, *129*, 7872–7876; *Angew. Chem. Int. Ed.* **2017**, *56*, 7764–7768.

[83] L. Zhang, P. Liang, H. B. Shu, X. L. Man, X. Q. Du, D. L. Chao, Z. G. Liu, Y. P. Sun, H. Z. Wan, H. Wang, *J. Colloid Interface Sci.* **2021**, *143*, 110849.

[84] P. B. Zhai, T. S. Wang, W. W. Yang, S. Q. Cui, P. Zhang, A. Nie, Q. Zhang, Y. J. Gong, *Adv. Energy Mater.* **2019**, *9*, 1804019–1804026.

[85] G. Huang, J. H. Han, F. Zhang, Z. Q. Wang, H. Kashani, K. Watanabe, M. W. Chen, *Adv. Mater.* **2019**, *31*, 1805334–1805341.

[86] H. Zhang, X. Liao, Y. Guan, Y. Xiang, M. Li, W. Zhang, X. Zhu, H. Ming, L. Lu, J. Qiu, Y. Huang, G. Cao, Y. Yang, L. Mai, Y. Zhao, *Nat. Commun.* **2018**, *9*, 359–367.

[87] Y. L. Wang, Y. B. Shen, Z. L. Du, X. F. Zhang, K. Wang, H. Y. Zhang, T. Kang, F. Guo, C. H. Liu, X. D. Wu, W. Lu, L. W. Chen, *J. Mater. Chem. A* **2017**, *5*, 23434–23439.

[88] Z. Sun, S. Jin, H. Jin, Z. Du, Y. Zhu, A. Cao, H. Ji, L. J. Wan, *Adv. Mater.* **2018**, *30*, 1800884–1800872.

[89] T. T. Zuo, X. W. Wu, C. P. Yang, Y. X. Yin, H. Ye, N. W. Li, Y. G. Guo, *Adv. Mater.* **2017**, *29*, 1700389–1700394.

[90] L. Liu, Y. X. Yin, J. Y. Li, N. W. Li, X. X. Zeng, H. Ye, Y. G. Guo, L. J. Wan, *Joule.* **2017**, *1*, 563–575.

[91] Q. Wang, C. K. Yang, J. J. Yang, K. Wu, L. Y. Qi, H. Tang, Z. Y. Zhang, W. Liu, H. H. Zhou, *Energy Storage Mater.* **2018**, *15*, 249–256.

[92] S. F. Liu, X. H. Xia, Z. J. Yao, J. B. Wu, L. Y. Zhang, S. J. Deng, C. G. Zhou, S. H. Shen, X. L. Wang, J. P. Tu, *Small Methods* **2018**, *2*, 1800035–1800042.

[93] L. Luo, J. Y. Li, H. Yaghoobnejad Asl, A. Manthiram, *Adv. Mater.* **2019**, *28*, 1904537.

[94] L. Liu, Y. X. Yin, J. Y. Li, S. H. Wang, Y. G. Guo, L. J. Wan, *Adv. Mater.* **2018**, *30*, 1706216.

[95] Y. Zhou, Y. Han, H. T. Zhang, D. Sui, Z. H. Sun, P. S. Xiao, X. T. Wang, Y. F. Ma, Y. S. Chen, *Energy Storage Mater.* **2018**, *14*, 222–229.

[96] Q. Wang, C. Yang, J. Yang, K. Wu, L. Qi, H. Tang, Z. Zhang, W. Liu, H. Zhou, *Energy Storage Mater.* **2018**, *15*, 249–256.

[97] Y. Zhang, C. W. Wang, G. Pastel, Y. D. Kuang, H. Xie, Y. J. Li, B. Y. Liu, W. Luo, C. Chen, L. B. Hu, *Adv. Energy Mater.* **2018**, *8*, 1800635–1800644.

[98] S. F. Ye, F. F. Liu, R. Xu, Y. Yao, X. F. Zhou, Y. Z. Feng, X. L. Cheng, Y. Yu, *Small.* **2019**, *15*, 1903725–1903732.

[99] F. F. Liu, Z. Z. Jin, Z. X. Hu, Z. W. Zhang, W. Liu, Y. Yu, *Chem. Asian J.* **2020**, *15*, 1057–1066.

[100] Y. Y. Liu, D. C. Lin, Z. Liang, J. Zhao, K. Yan, Y. Cui, *Nat. Commun.* **2016**, *7*, 10992–11000.

[101] X. Y. Yue, J. Bao, S. Y. Yang, R. J. Luo, Q. C. Wang, X. J. Wu, Z. Shadike, X. Q. Yang, Y. N. Zhou, *Nano Energy.* **2020**, *71*, 104614–104623.

[102] W. Go, M. H. Kim, J. Park, C. H. Lim, S. H. Joo, Y. Kim, H. W. Lee, *Nano Lett.* **2019**, *19*, 1504–1511.

[103] H. Yang, R. Xu, Y. Gong, Y. Yao, L. Gu, Y. Yu, *Nano Energy.* **2018**, *48*, 448–455.

[104] Y. Yu, C. H. Chen, J. L. Shui, S. Xie, *Angew. Chem. Int. Ed.* **2005**, *44*, 7085–7089; *Angew. Chem.* **2005**, *117*, 7247–7251.

[105] M. Zhang, L. Xiang, M. Galluzzi, C. L. Jiang, S. Q. Zhang, J. Y. Li, Y. B. Tang, *Adv. Mater.* **2019**, *31*, 1900826–1900832.

[106] K. R. Adair, M. Iqbal, C. Wang, Y. Zhao, M. N. Banis, R. Li, L. Zhang, R. Yang, S. Lu, X. Sun, *Nano Energy.* **2018**, *54*, 375–382.

[107] H. Qiu, T. Tang, M. Asif, X. Huang, Y. Hou, *Adv. Funct. Mater.* **2019**, *29*, 1808468–1808473.

[108] Q. Yun, Y. B. He, W. Lv, Y. Zhao, B. Li, F. Kang, Q. H. Yang, *Adv. Mater.* **2016**, *28*, 6932–6939.

[109] P. L. Li, X. L. Dong, C. Li, J. Y. Liu, Y. Liu, W. L. Feng, C. X. Wang, Y. G. Wang, Y. Y. Xia, *Angew. Chem. Int. Ed.* **2019**, *58*, 2093–2097; *Angew. Chem.* **2019**, *131*, 2115–2119.

[110] S. S. Chi, Y. Liu, W. L. Song, L. Z. Fan, Q. Zhang, *Adv. Funct. Mater.* **2017**, *27*, 1700348–1700357.

[111] Y. Zhou, K. Zhao, Y. Han, Z. H. Sun, H. T. Zhang, L. Q. Xu, Y. F. Ma, Y. S. Chen, *J. Mater. Chem. A* **2019**, *7*, 5712–5718.

[112] Z. J. Huang, C. Zhang, W. Lv, G. M. Zhou, Y. B. Zhang, Y. Q. Deng, H. L. Wu, F. Y. Kang, Q. H. Yang, *J. Mater. Chem. A* **2019**, *7*, 727–732.

[113] G. H. Yang, J. D. Chen, P. T. Xiao, P. O. Agboola, I. Shakir, Y. X. Xu, *J. Mater. Chem. A* **2018**, *6*, 9899–9905.

[114] X. Y. Yue, W. W. Wang, Q. C. Wang, J. K. Meng, Z. Q. Zhang, X. J. Wu, X. Q. Yang, Y. N. Zhou, *Energy Storage Mater.* **2018**, *14*, 335–344.

[115] X. Ke, Y. H. Liang, L. H. Ou, H. D. Liu, Y. M. Chen, W. Wu, Y. F. Cheng, Z. P. Guo, Y. Q. Lai, P. Liu, Z. Shi, *Energy Storage Mater.* **2019**, *23*, 547–555.

[116] F. H. Ren, Z. Y. Lu, H. Zhang, L. Y. Huai, X. C. Chen, S. D. Wu, Z. Peng, D. Y. Wang, J. C. Ye, *Adv. Funct. Mater.* **2018**, *28*, 1805638–1805649.

[117] Y. Liu, X. Qin, S. Zhang, L. Zhang, F. Kang, G. Chen, X. Duan, B. Li, *J. Mater. Chem. A* **2019**, *7*, 13225–13233.

[118] C. P. Yang, Y. X. Yin, S. F. Zhang, N. W. Li, Y. G. Guo, *Nat. Commun.* **2015**, *6*, 9058–9066.

[119] S. H. Wang, Y. X. Yin, T. T. Zuo, W. Dong, J. Y. Li, J. L. Shi, C. H. Zhang, N. W. Li, C. J. Li, Y. G. Guo, *Adv. Mater.* **2017**, *29*, 1703729–1703736.

[120] S. L. Wu, Z. Y. Zhang, M. H. Lan, S. R. Yang, J. Y. Cheng, J. J. Cai, J. H. Shen, Y. Zhu, K. L. Zhang, W. J. Zhang, *Adv. Mater.* **2018**, *30*, 1705830–1705836.

[121] Y. L. An, H. F. Fei, G. F. Zeng, X. Y. Xu, L. J. Ci, B. J. Xi, S. L. Xiong, J. K. Feng, Y. T. Qian, *Nano Energy* **2018**, *47*, 503–511.

[122] H. Ye, Z. J. Zheng, H. R. Yao, S. C. Liu, T. T. Zuo, X. W. Wu, Y. X. Yin, N. W. Li, J. J. Gu, F. F. Cao, Y. G. G, *Angew. Chem. Int. Ed.* **2019**, *58*, 1094–1099; *Angew. Chem.* **2019**, *131*, 1106–1111.

Batteries & Supercaps

Review

doi.org/10.1002/batt.202200231

Chemistry
Europe

European Chemical
Societies Publishing

[123] T. H. Xu, P. Gao, P. R. Li, K. Xia, N. Han, J. Deng, Y. G. Li, J. Lu, *Adv. Energy Mater.* **2020**, *10*, 1902343–1902348.

[124] Y. Ouyang, C. Cui, Y. P. Guo, Y. Q. Wei, T. Y. Zhai, H. Q. Li, *ACS Appl. Mater. Interfaces* **2020**, *12*, 25818–25825.

[125] Z. Tu, S. Choudhury, M. J. Zachman, S. Wei, K. Zhang, L. F. Kourkoutis, L. A. Archer, *Nat. Energy.* **2018**, *3*, 310–316.

[126] Z. J. Zheng, Q. Su, Q. Zhang, X. C. Hu, Y. X. Yin, R. Wen, H. Ye, Z. B. Wang, Y. G. Guo, *Nano Energy* **2019**, *64*, 103910–103917.

[127] F. F. Liu, Z. W. Zhang, S. F. Ye, Y. Yao, Y. Yan, *Acta Phys.-Chim.* **2021**, *37*, 2006021.

[128] W. H. Li, S. H. Hu, X. Y. Luo, Z. L. Li, X. Z. Sun, M. S. Li, F. F. Liu, Y. Yu, *Adv. Mater.* **2017**, *29*, 1605820.

[129] M. Q. Zhu, B. Li, S. M. Li, Z. G. Du, Y. J. Gong, S. B. Yang, *Adv. Energy Mater.* **2018**, *8*, 1703505–1703511.

[130] T. S. Wang, X. Liu, X. Zhao, P. He, C. W. Nan, L. Z. Fan, *Adv. Funct. Mater.* **2020**, *30*, 2000786–2000795.

[131] J. Qian, Y. Li, M. L. Zhang, R. Luo, F. J. Wang, Y. S. Ye, Y. Xing, W. L. Li, W. J. Qu, L. L. Wang, Y. J. Li, F. Wu, R. J. Chen, *Nano Energy* **2019**, *60*, 866–874.

[132] T. C. Liu, J. L. Wang, Y. Xu, Y. F. Zhang, Y. Wang, *Nano-Micro Lett.* **2021**, *30*, 170–182.

[133] Y. L. Jie, X. D. Ren, R. G. Cao, W. B. Cai, S. H. Jiao, *Adv. Funct. Mater.* **2020**, *30*, 1910777–1910799.

[134] S. M. Wang, J. Y. Qu, F. Wu, K. Yan, C. Z. Zhang, *ACS Appl. Mater. Interfaces* **2020**, *12*, 8366–8375.

[135] L. F. Xiao, Z. Q. Zeng, X. W. Liu, Y. J. Fang, X. Y. Jiang, Y. Y. Shao, L. Zhuang, X. P. Ai, H. X. Yang, Y. L. Cao, J. Liu, *ACS Energy Lett.* **2019**, *4*, 483–488.

[136] B. Liu, W. Xu, P. F. Yan, S. T. Kim, M. H. Engelhard, X. L. Sun, D. H. Mei, J. Cho, C. M. Wang, J. G. Zhang, *Adv. Energy Mater.* **2017**, *7*, 1770074–1770075.

[137] W. J. Chen, B. Q. Li, C. X. Zhao, M. Zhao, T. Q. Yuan, R. C. Sun, J. Q. Huang, Q. Zhang, *Angew. Chem. Int. Ed.* **2020**, *59*, 10732–10745; *Angew. Chem.* **2020**, *132*, 10821–10834.

[138] J. Zheng, J. A. Lochala, A. Kwok, Z. D. Deng, J. Xiao, *Adv. Sci.* **2017**, *4*, 1700032–170041.

[139] B. Liu, W. Xu, P. F. Yan, X. L. Sun, M. E. Bowden, J. Read, J. F. Qian, D. H. Mei, C. M. Wang, J. G. Zhang, *Adv. Funct. Mater.* **2016**, *26*, 605–613.

[140] L. Yu, S. R. Chen, H. Lee, L. C. Zhang, M. H. Engelhard, Q. Y. Li, S. H. Jiao, J. Liu, W. Xu, J. G. Zhang, *ACS Energy Lett.* **2018**, *3*, 2059–2067.

[141] J. F. Qian, W. A. Henderson, W. Xu, P. Bhattacharya, M. Engelhard, O. Borodin, J. G. Zhang, *Nat. Commun.* **2015**, *6*, 1518–1534.

[142] K. Matsumoto, K. Inoue, K. Nakahara, R. Yuge, T. Noguchi, K. Utsugi, *J. Power Sources* **2013**, *231*, 234–238.

[143] X. Dong, Y. Lin, P. Li, Y. Ma, J. Huang, D. Bin, Y. Wang, Y. Qi, Y. Xia, *Angew. Chem. Int. Ed.* **2019**, *58*, 5623–5627; *Angew. Chem.* **2019**, *131*, 5679–5683.

[144] A. Rafie, J. Kim, K. Sarode, V. Kalra, *Energy Storage Mater.* **2022**, *50*, 197–224.

[145] S. Yuan, T. Kong, Y. Zhang, P. Dong, Y. Zhang, X. Dong, Y. Wang, Y. Xia, *Angew. Chem.* **2021**, *133*, 25828–25842.

[146] Z. Peng, X. Cao, P. Gao, H. Jia, X. Ren, S. Roy, Z. Li, Y. Zhu, W. Xie, D. Liu, Q. Li, D. Wang, W. Xu, J-G. Zhang, *Adv. Funct. Mater.* **2020**, *30*, 2001285–2001289.

[147] R. Miao, J. Yang, Z. Xu, J. Wang, Y. Nuli, L. Sun, *Sci. Rep.* **2016**, *6*, 21771–21776.

[148] H. H. Sun, A. Dolocan, J. A. Weeks, R. Rodriguez, A. Heller, C. B. J. Mullins, *J. Mater. Chem. A* **2019**, *30*, 17782–17789.

[149] C. Li, L. Gu, J. Maier, *Adv. Funct. Mater.* **2012**, *22*, 1145–1149.

[150] A. M. Haregewoin, A. S. Wotango, B. Hwang, *Energy Environ. Sci.* **2016**, *9*, 1955–1988.

[151] H. J. Zhao, X. Q. Yu, J. D. Li, B. Li, H. Y. Shao, L. Li, Y. H. Deng, *J. Mater. Chem. A* **2019**, *7*, 8700–8722.

[152] R. McMillan, H. Slegr, Z. X. Shu, W. D. Wang, *J. Power Sources* **1999**, *81*, 20–26.

[153] I. A. Profatilova, S. S. Kim, N. S. Choi, *Electrochim. Acta* **2009**, *54*, 4445–4450.

[154] A. Rezqita, M. Sauer, A. Foelske, H. Kronberger, A. Trifonova, *Electrochim. Acta* **2017**, *247*, 600–609.

[155] X. Q. Zhang, X. B. Cheng, X. Chen, C. Yan, Q. Zhang, *Adv. Funct. Mater.* **2017**, *27*, 1605989–1605996.

[156] O. Matsuoka, A. Hiwara, T. Omi, M. Toriida, T. Hayashi, C. Tanaka, Y. Saito, T. Ishida, H. Tan, S. S. Ono, S. Yamamoto, *J. Power Sources* **2002**, *108*, 128–138.

[157] E. G. Leggesse, J. C. Jiang, *J. Phys. Chem. A* **2012**, *116*, 11025–11033.

[158] F. Ren, W. Zuo, X. Yang, M. Lin, L. Xu, W. Zhao, S. Zheng, Y. Yang, *J. Phys. Chem. C* **2019**, *123*, 5871–5880.

[159] S. S. Zhang, *Electrochim. Acta* **2012**, *70*, 344–348.

[160] X. D. Ren, Y. H. Zhang, M. H. Engelhard, Q. Y. Li, J. G. Zhang, W. Xu, *ACS Energy Lett.* **2018**, *3*, 14–19.

[161] H. Xiang, P. Shi, P. Bhattacharya, X. Chen, D. Mei, M. E. Bowden, J. Zheng, J. G. Zhang, W. J. Xu, *J. Power Sources* **2016**, *318*, 170–177.

[162] S. Y. Li, D. N. Zhao, P. Wang, X. L. Cui, F. J. Tang, *Electrochim. Acta.* **2016**, *222*, 668–677.

[163] C. Yan, X. B. Cheng, C. Z. Zhao, J. Q. Huang, S. T. Yang, Q. J. Zhang, *J. Power Sources.* **2016**, *327*, 212–220.

[164] Z. M. Huang, J. Ren, W. Zhang, M. L. Xie, Y. K. Li, D. Sun, Y. Shen, Y. H. Huang, *Adv. Mater.* **2018**, *30*, 1803270–1803275.

[165] J. Zheng, M. H. Engelhard, D. Mei, S. Jiao, B. J. Polzin, J. G. Zhang, W. Xu, *Nat. Energy* **2017**, *2*, 961–969.

[166] J. Meng, F. Chu, J. Hu, C. Li, *Adv. Funct. Mater.* **2019**, *29*, 1902220.

[167] Y. Zhao, Y. Ye, F. Wu, Y. Li, L. Li, R. Chen, *Adv. Mater.* **2019**, *22*, 1806532–1806548.

[168] C. Z. Zhao, X. B. Cheng, R. Zhang, H. J. Peng, J. Q. Huang, R. Ran, Z. H. Huang, F. Wei, Q. Zhang, *Energy Storage Mater.* **2016**, *3*, 77–83.

[169] G. Li, Y. Gao, X. He, Q. Huang, S. Chen, S. H. Kim, D. Wang, *Nat. Commun.* **2017**, *8*, 850–859.

[170] G. Li, Q. Huang, X. He, Y. Gao, D. Wang, S. H. Kim, D. Wang, *ACS Nano* **2018**, *12*, 1500–1507.

[171] T. Wang, Y. Li, J. Zhang, K. Yan, P. Jaumaux, J. Yang, C. Wang, D. Shanmukaraj, B. Sun, M. Armand, Y. Cui, G. Wang, *Nat. Commun.* **2020**, *11*, 5429.

[172] J. R. Wu, X. S. Wang, Q. Liu, S. W. Wang, D. Zhou, F. Y. Kang, D. Shanmukaraj, M. Armand, T. Rojo, B. H. Li, G. X. Wang, *Nat. Commun.* **2021**, *30*, 5746.

[173] Z. Gao, H. Sun, L. Fu, F. Ye, Y. Zhang, W. Luo, Y. Huang, *Adv. Mater.* **2018**, *30*, 1870122–1870123.

[174] H. Yang, C. Guo, A. Naveed, J. Lei, J. Yang, Y. Nuli, J. Wang, *Energy Storage Mater.* **2018**, *14*, 199–221.

[175] J. Hou, X. Tu, X. Wu, M. Shen, X. Wang, C. Wang, C. Cao, H. Pang, G. Wang, *Chem. Eng. J.* **2020**, *401*, 126141–126151.

[176] J. Chen, J. Wu, X. Wang, A. Zhou, Z. Yang, *Energy Storage Mater.* **2021**, *35*, 70–87.

[177] H. Zhang, C. Li, M. Piszcz, E. Coya, T. Rojo, L. M. RodriguezMartinez, M. Armand, Z. Zhou, *Chem. Soc. Rev.* **2017**, *46*, 797–815.

[178] W. H. Meyer, *Adv. Mater.* **1998**, *10*, 439–448.

[179] A. Manuel Stephan, K. S. Nahm, *Polymer.* **2006**, *47*, 5952–5964.

[180] E. Quartarone, P. Mustarelli, *Chem. Soc. Rev.* **2011**, *40*, 2525–2540.

[181] D. Zhou, A. Tkacheva, X. Tang, B. Sun, D. Shanmukaraj, P. Li, F. Zhang, M. Armand, G. Wang, *Angew. Chem. Int. Ed.* **2019**, *58*, 6001–6006; *Angew. Chem.* **2019**, *131*, 6062–6067.

[182] Z. Deng, Z. Wang, I. H. Chu, J. Luo, S. P. Ong, *Electrochem.Soc.* **2016**, *163*, A67–A74.

[183] G. M. Stone, S. A. Mullin, A. A. Teran, D. T. Hallinan Jr., A. M. Minor, A. Hexemer, N. P. Balsara, *J. Electrochem. Soc.* **2011**, *159*, A222–A227.

[184] Y. Zhu, X. He, Y. Mo, *ACS Appl. Mater. Interfaces* **2015**, *7*, 23685–23693.

[185] N. B. Aetukuri, S. Kitajim, E. Jung, L. E. Thompson, K. Virwani, M. L. Reich, M. Kunze, M. Schneider, W. Schmidbauer, W. W. Wilcke, D. S. Bethune, J. C. Scott, R. D. Miller, H. C. Kim, *Adv. Energy Mater.* **2015**, *5*, 1500265–1500270.

[186] W. Zhou, S. Wang, Y. Li, S. Xin, A. Manthiram, *Am. Chem.* **2016**, *138*, 9385–9388.

[187] X. W. Yu, J. Y. Li, A. Manthiram, *ACS Materials Lett.* **2020**, *2*, 317–324.

[188] J. Duan, W. Y. Wu, A. M. Nolan, T. R. Wang, J. Y. Wen, C. C. Hu, Y. F. Mo, W. Luo, Y. H. Huang, *Adv. Mater.* **2019**, *31*, 1807243–1807249.

[189] A. Wang, S. Madam, H. Li, S. Shi, Y. Qi, *NPJ Comput. Mater.* **2018**, *4*, 359–367.

[190] S. Lv, T. Verhallen, A. Vasileiadis, F. Ooms, Y. Xu, Z. Li, M. Wagemaker, *Nat. Commun.* **2018**, *9*, 2152–2157.

[191] S. M. Bak, Z. Shadike, R. Lin, X. Yu, X. Q. Yang, *NPG Asia Mater.* **2018**, *10*, 563–580.

[192] H. C. Gao, N. S. Grundish, Y. J. Zhao, A. J. Zhou, J. B. Goodenough, *Adv. Energy Mater.* **2021**, *1*, 1932952–1932962.

[193] J. Lee, D. A. Kitchaev, D. H. Kwon, C. W. Lee, J. K. Papp, Y. S. Liu, Z. Lun, R. J. Clement, T. Shi, B. D. McCloskey, J. Guo, M. Balasubramanian, G. Ceder, *Nature* **2018**, *556*, 185–190.

[194] G. Yang, S. Frisco, R. Tao, N. Philip, T. H. Bennett, C. Stetson, J. G. Zhang, S. D. Han, G. Teeter, S. P. Harvey, Y. Zhang, G. M. Veith, J. Nanda, *ACS Energy Lett.* **2021**, *6*, 1684–1693.

[195] L. Shi, A. Xu, T. Zhao, *ACS Appl. Mater. Interfaces* **2017**, *9*, 1987–1994.

[196] X. Q. Zhang, X. B. Cheng, Q. Zhang, *Adv. Mater. Interfaces* **2018**, *5*, 1701097–1701115.

[197] R. Xu, X. B. Cheng, C. Yan, X. Q. Zhang, Y. Xiao, C. Z. Zhao, J. Q. Zhang, Q. Zhang, *Matter* **2019**, *1*, 317–344.

[198] D. C. Lin, Y. Y. Liu, W. Chen, G. M. Zhou, K. Liu, B. Dunn, Y. Cui, *Nano Lett.* **2017**, *17*, 3731–3737.

[199] J. Zhao, L. Liao, F. Shi, T. Lei, G. Chen, A. Pei, J. Sun, K. Yan, G. Zhou, J. Xie, C. Liu, Y. Li, Z. Liang, Z. Bao, Y. Cui, *J. Am. Chem. Soc.* **2017**, *139*, 11550–11558.

[200] C. Yan, X. B. Cheng, Y. X. Yao, X. Shen, B. Q. Li, W. J. Li, R. Zhang, J. Q. Huang, H. Li, Q. Zhang, *Adv. Mater.* **2018**, *30*, 1804461.

[201] X. Liang, Q. Pang, I. R. Kochetkov, M. S. Sempere, H. Huang, X. Sun, L. F. Nazar, *Nat. Energy* **2017**, *2*, 652–657.

[202] L. Wang, S. Fu, T. Zhao, J. Qian, N. Chen, L. Li, F. Wu, R. Chen, *J. Mater. Chem. A* **2020**, *8*, 1247–1253.

[203] Z. Peng, N. Zhao, Z. Zhang, H. Wan, H. Lin, M. Liu, C. Shen, H. He, X. Guo, J. G. Zhang, D. Wang, *Nano Energy* **2017**, *39*, 662–672.

[204] Y. Zhang, G. Wang, L. Tang, J. Wu, B. Guo, M. Zhu, C. Wu, S. X. Dou, M. Wu, *J. Mater. Chem. A* **2019**, *7*, 25369–25376.

[205] G. Wang, X. Xiong, D. Xie, X. Fu, Z. Lin, C. Yang, K. Zhang, M. Liu, *ACS Appl. Mater. Interfaces* **2019**, *11*, 4962–4968.

[206] G. Li, Q. Huang, X. He, Y. Gao, D. Wang, S. H. Kim, D. Wang, *ACS Nano.* **2018**, *12*, 1500–1507.

[207] F. F. Liu, L. F. Wang, Z. W. Zhang, P. C. Shi, Y. Z. Feng, Y. Yao, S. F. Ye, H. Y. Wang, X. J. Wu, Y. Yu, *Adv. Funct. Mater.* **2020**, *30*, 2001607–2001615.

[208] R. Xu, X. Q. Zhang, X. B. Cheng, H. J. Peng, C. Z. Zhao, C. Yan, J. Q. Huang, *Adv. Funct. Mater.* **2018**, *28*, 1705838–1705846.

[209] J. Luo, C. C. Fang, N. L. Wu, *Adv. Energy Mater.* **2018**, *8*, 1701482–1701488.

[210] B. Zhu, Y. Jin, X. Hu, Q. Zheng, S. Zhang, Q. Wang, J. Zhu, *Adv. Mater.* **2017**, *29*, 1603755–1603760.

[211] G. Wang, C. Chen, Y. Chen, X. Kang, C. Yang, F. Wang, Y. Liu, X. Xiong, *Angew. Chem. Int. Ed.* **2020**, *59*, 2055–2060; *Angew. Chem.* **2020**, *132*, 2071–2076.

[212] G. Li, Y. Gao, X. He, Q. Huang, S. Chen, S. H. Kim, D. Wang, *Nat. Commun.* **2017**, *8*, 850–858.

[213] G. Li, Q. Huang, X. He, Y. Gao, D. Wang, S. H. Kim, *ACS Nano* **2018**, *12*, 1500–1507.

[214] N. W. Li, Y. Shi, Y. X. Yin, X. X. Zeng, J. Y. Li, C. J. Li, L. J. Wan, R. Wen, Y. G. Guo, *Angew. Chem. Int. Ed.* **2018**, *57*, 1505–1509; *Angew. Chem.* **2018**, *130*, 1521–1525.

[215] Z. Jiang, L. Jin, Z. Han, W. H. Zeng, Y. Sun, J. Xie, *Angew. Chem. Int. Ed.* **2019**, *131*, 11496–11500.

[216] F. Lee, M. C. Tsai, M. H. Lin, Y. L. Ni'mah, S. Hy, C. Y. Kuo, J. H. Cheng, J. Rick, W. N. Su, B. J. Hwang, *J. Mater. Chem. A.* **2017**, *5*, 6708–6715.

[217] W. Liu, W. Li, D. Zhuo, G. Zheng, Z. Lu, K. Liu, Y. Cui, *ACS Cent. Sci.* **2017**, *3*, 135–140.

[218] J. H. Kim, H. S. Woo, W. K. Kung, K. H. Ryu, D. W. Kim, *ACS Appl. Mater. Interfaces* **2016**, *8*, 32300–32306.

[219] H. Chen, A. Pei, D. Lin, J. Xie, A. Yang, J. Xu, K. Lin, J. Wang, H. Wang, F. Shi, D. Boyle, Y. Cui, *Adv. Energy Mater.* **2019**, *9*, 1900858–1900865.

[220] P. Li, X. Dong, C. Li, J. Liu, Y. Liu, W. Feng, C. Wang, Y. Wang, Y. Xia, *Angew. Chem. Int. Ed.* **2019**, *58*, 2093–2097; *Angew. Chem.* **2019**, *131*, 2115–2119.

[221] X. Wang, W. Zeng, L. Hong, W. Xu, H. Yang, F. Wang, H. Duan, M. Tang, H. Jiang, *Nat. Energy* **2018**, *3*, 227–235.

[222] X. Y. Yue, X. L. Li, J. Bao, Q. Q. Qiu, T. Liu, D. Chen, S. S. Yuan, X. J. Wu, J. Lu, Y. N. Zhou, *Adv. Energy Mater.* **2019**, *9*, 1901491.

[223] Y. Chen, M. Yue, C. Liu, H. Zhang, Y. Yu, X. Li, H. Zhang, *Adv. Funct. Mater.* **2019**, *29*, 1806752.

[224] J. Liu, Z. Bao, Y. Cui, E. J. Dufek, J. B. Goodenough, P. Khalifah, Q. Li, B. Liaw, P. Liu, A. Manthiram, Y. Meng, V. Subramanian, M. Toney, V. Viswanathan, M. Whittingham, J. Xiao, W. Xu, J. Yang, X. Yang, J. G. Zhang, *Nat. Energy* **2019**, *4*, 180–186.

[225] A. Etxebarria, S. L. Koch, O. Bondarchuk, S. Passerini, G. Teobaldi, M. A. Munoz-Marquez, *Adv. Energy Mater.* **2020**, *10*, 2000520.

[226] R. Xu, X. B. Cheng, C. Yan, X. Q. Zhang, Y. Xiao, C. Z. Zhao, J. Q. Huang, Q. Zhang, *Matter.* **2019**, *1*, 317–344.

[227] S. Qu, W. Jia, Y. Wang, C. Li, Z. Yao, K. Li, Y. Liu, W. Zou, F. Zhou, Z. Wang, J. Li, *Electrochim. Acta* **2019**, *317*, 120–127.

[228] Y. Ma, P. W. Qi, J. Ma, L. Wei, L. Zhao, J. Cheng, Y. H. Su, Y. T. Gu, Y. B. Lian, Y. Peng, Y. B. Shen, L. W. Chen, Z. Deng, Z. F. Liu, *Adv. Sci.* **2020**, *23*, 200520.

[229] J. Wang, H. H. Hua, J. Zhang, L. Li, L. J. Jia, Q. H. Guan, H. F. Hu, H. T. Liu, Y. F. Jia, Q. Zhuang, S. Cheng, M. Huang, H. Z. Lin, *Energy Storage Mater.* **2022**, *52*, 210–219.

[230] Y. Y. Wang, Z. J. Wang, L. Zhao, Q. Fan, X. H. Zeng, S. L. Liu, W. K. Pang, Y. B. He, Z. P. Guo, *Adv. Mater.* **2021**, *33*, 2008133.

[231] K. Yan, J. Wang, S. Zhao, D. Zhou, B. Sun, Y. Cui, G. Wang, *Angew. Chem. Int. Ed.* **2019**, *58*, 11364–11368; *Angew. Chem.* **2019**, *131*, 11486–11490.

[232] J. Xiao, Q. Li, Y. Bi, M. Cai, B. Dunn, T. Glossmann, J. Liu, T. Osaka, R. Sugiura, B. Wu, J. Yang, J. G. Zhang, M. S. Whittingham, *Nat. Energy* **2020**, *5*, 561–568.

[233] K. R. Adair, M. N. Banis, Y. Zhao, T. Bond, R. Li, X. Sun, *Adv. Mater.* **2020**, *32*, 2002550.

[234] L. P. Hou, X. Q. Zhang, B. Q. Li, Q. Zhang, *Angew. Chem. Int. Ed.* **2020**, *132*, 15221–15225.